Petrologic Significance of Multiple Magmas in the Quottoon Igneous Complex, NW British Columbia and SE Alaska

by

Jay B. Thomas

Petrogenesis, Isotope Geology, and Tectonics Laboratory

Thesis submitted to the Faculty of the

Virginia Polytechnic Institute and State University

in partial fulfillment of the requirements for the Master of Science Degree

in

Department of Geological Sciences

APPROVED BY:

A. Krishna Sinha, Chairman

James S. Beard

Maria L. Crawford

May, 1998

Blacksburg, Virginia

Key words: Quottoon pluton, quartz diorite, tonalite, magma, British Columbia, Alaska, petrography, major elements, trace elements, rare earth elements, geochemistry, Sr isotopes, geochemical modeling, Great Tonalite Sill

Petrologic Significance of Multiple Magmas in the Quottoon Igneous Complex, NW British Columbia and SE Alaska

by

Jay B. Thomas

A. Krishna Sinha, Chairman

Petrogenesis, Isotope Geology, and Tectonics Laboratory

Department of Geological Sciences

(ABSTRACT)

The quartz dioritic Quottoon Igneous Complex (QIC) is a major Paleogene (65-56 Ma) magmatic body in NW British Columbia and SE Alaska that was emplaced along the Coast shear zone (CSZ). The QIC contains two different igneous suites that provide information about source regions, magmatic processes and evolving tectonic regimes that changed from a dominantly convergent to a dominantly strike-slip regime between 65 to 55 Ma. Heterogeneous suite I rocks (e. g. along Steamer Passage) have a pervasive solid-state fabric, abundant mafic enclaves and dikes, metasedimentary screens, and variable color indices (25-50). The homogeneous suite II rocks (e. g. along Quottoon Inlet) have a weak (to absent) fabric developed in the magmatic state (aligned feldspars, melt filled shears), and more uniform color indices (24-34) than in suite I. Suite I rocks have Sr concentrations <750 ppm, avg. La_N/Yb_N = 10.4, and initial $^{87}Sr/^{86}Sr$ ratios that range from 0.70513 to 0.70717. The suite II rocks have Sr concentrations >750 ppm, avg. La_N/Yb_N = 23.1, and initial $^{87}Sr/^{86}Sr$ ratios that range from 0.70617 to 0.70686. This study proposes that the parental QIC magma (initial $^{87}Sr/^{86}Sr$ = 0.706) can be derived bypartial melting of an amphibolitic source reservoir at lower crustal conditions. Geochemical data (Rb, Sr, Ba and La_N/Yb_N) and initial $^{87}Sr/^{86}Sr$ ratios preclude linkages between

the two suites by fractional crystallization or assimilation and fractional crystallization (AFC) processes. The suite I rocks are interpreted to be the result of magma mixing between the QIC parental magma and a mantle derived magma. The samples do not lie along a single mixing line due to continued evolution through fractional crystallization/AFC processes subsequent to magma mixing. The suite II rocks may be generated by AFC. Initial $^{87}Sr/^{86}Sr$ ratio data suggests that similar processes to those that affected the QIC may also have operated during the generation of other portions of the Great Tonalite Sill of southeast Alaska.

Acknowledgements

I would like to thank all those who urged me to fulfill my potential at an early age even when I behaved quite stubbornly. It was my parents to whom I owe the most thanks for they were the ones who put up with my hard headed ways and continued to love me even when I behaved worse than most of those who know me now can imagine. I should also thank those at Guilford College who truly were the ones that inspired me to continue in my geological education. The memories of many field trips through the Appalachians with Charles Almy, Cyril Harvey, and Marlene McCauley will remain engraved in my mind forever. It was on these trips where I really learned about the earth.

This work was supported by the National Science Foundation Grant EAR 9526613 as part of the consortium "ACCRETE" project. I would like to thank A. Krishna Sinha for spending endless hours debating the science with me. He provided as much time as was necessary, even on the weekends, to teach me the many laboratory procedures that were required to complete this project. I also need to thank Maria Luisa Crawford for spending the summer of 1996 with me doing field work in the ruggedly beautiful mountains of northwestern British Columbia and southeastern Alaska. She provided tremendous geological insight and taught me much about doing field work. William Crawford and Rick Matthews were instrumental in keeping me sane in the field (by taking me fishing) as well as taking me to the most beautiful places that I have ever seen via boat. James Beard taught me the details of partial melting and also offered me much of his personal time to talk about earthly processes. Hal Pendrak was always helpful and enthusiastic about my questions, even when I told him that I was having a problem running one kind of machine or another.

The perseverance to complete this project came from those that I worked closely with in the PIT lab including Court, Mona, Kimball, Jin, and Jim. I have benefited from their scientific knowledge and integrity. I also need to thank Aus, Brian, and Amy from the carbonate lab for enduring my frequent visits to escape the drone of the PIT lab. My roommates John, Mike, Adam, Eric, Jim, Peter, Luca, and Eddie have tolerated me over the past years. My best friend Jay W. has also helped keep me sane throughout this portion of my life by using the old-fashioned smallmouth bass remedy in the summer and the trout remedy in the winter.

Table of Contents

List of Illustrations

List of Tables

Introduction

The Quottoon pluton is an elongate, sheet-like body of quartz diorite located in northwest British Columbia and southeast Alaska and is part of the Coast Plutonic Complex (Hutchison, 1982). It is considered to be the southern terminus of the late Cretaceous to Eocene Great Tonalite Sill (Brew and Ford, 1978; Kenah, 1979; Gehrels et al., 1991; Ingram, 1991; Brew, 1994). The orogen-parallel collection of plutons that comprise the Great Tonalite Sill is ~1000 km long and <25 km wide. It stretches from north of Juneau, Alaska to the headwaters of the Kowease River at 53°00 N in British Columbia (fig. 1a) (Armstrong and Runkle, 1979; Kenah, 1979; Hutchison, 1982; Drinkwater et al., 1989, 1990; Arth et al., 1989; Van der Heyden, 1989; Gareau, 1991; Ingram, 1992). In NW British Columbia and SE Alaska, the Quottoon pluton intruded in close proximity to a major structural discontinuity, the Coast shear zone (CSZ) (fig. 1b) (Crawford et al., 1987; Crawford, 1995). The CSZ has been variably interpreted as a suture between the Stikine terrane and the outboard Wrangellia/Alexander terranes (Monger et al., 1982, 1983, 1993; Crawford et al., 1987) or as an intraplate rift along which magmas of the Great Tonalite Sill were emplaced (Brew and Ford, 1983; Gehrels et al., 1988). Regardless of the tectonic interpretation, it is agreed that the CSZ provided a zone of structural weakness to the Quottoon pluton and associated plutons of the Great Tonalite Sill belt (Brew and Ford 1981, 1983; Gehrels et al., 1991b; Ingram, 1992). The CSZ has been interpreted as evolving from a dominantly convergent to a weakly strike-slip feature contemporaneous with magma generation and emplacement of the Quottoon pluton (Klepeis and Crawford, 1996).

New field observations, petrologic, and isotopic data from five transects across the Quottoon pluton are presented to better constrain the dominant petrologic processes responsible for its generation and subsequent magmatic evolution. Published major element geochemical data for the Quottoon pluton (Hutchison, 1982) combined with recent field and geochemical evidence demonstrate the occurrence of distinct magmatic suites within the Quottoon pluton (fig. 1b) (Sinha and Thomas, 1996; Thomas and Sinha, 1997; Thomas, 1998). A distinct structural and geochemical boundary across strike indicates that the Quottoon pluton is indeed an igneous complex (the Quottoon Igneous Complex (QIC)) composed of physically and chemically distinct magmas emplaced in close spatial association (fig. 1b). Likewise, interpretation of published data from other plutons of the Great Tonalite Sill (along strike) suggests that similar igneous

suites may be present in the Speel River, Annex Lakes, and Carlson Creek plutons (Drinkwater et al., 1989, 1990, 1995; Gehrels et al., 1991). This study utilizes field, petrographic, geochemical, and Sr isotopic data to resolve the dominant igneous processes (fractional, crystallization, assimilation and fractional crystallization, or magma mixing) responsible for the distinct magmatic suites of the QIC. A thorough understanding of the QIC may provide some insight into the petrogenesis of other plutons of the GTS.

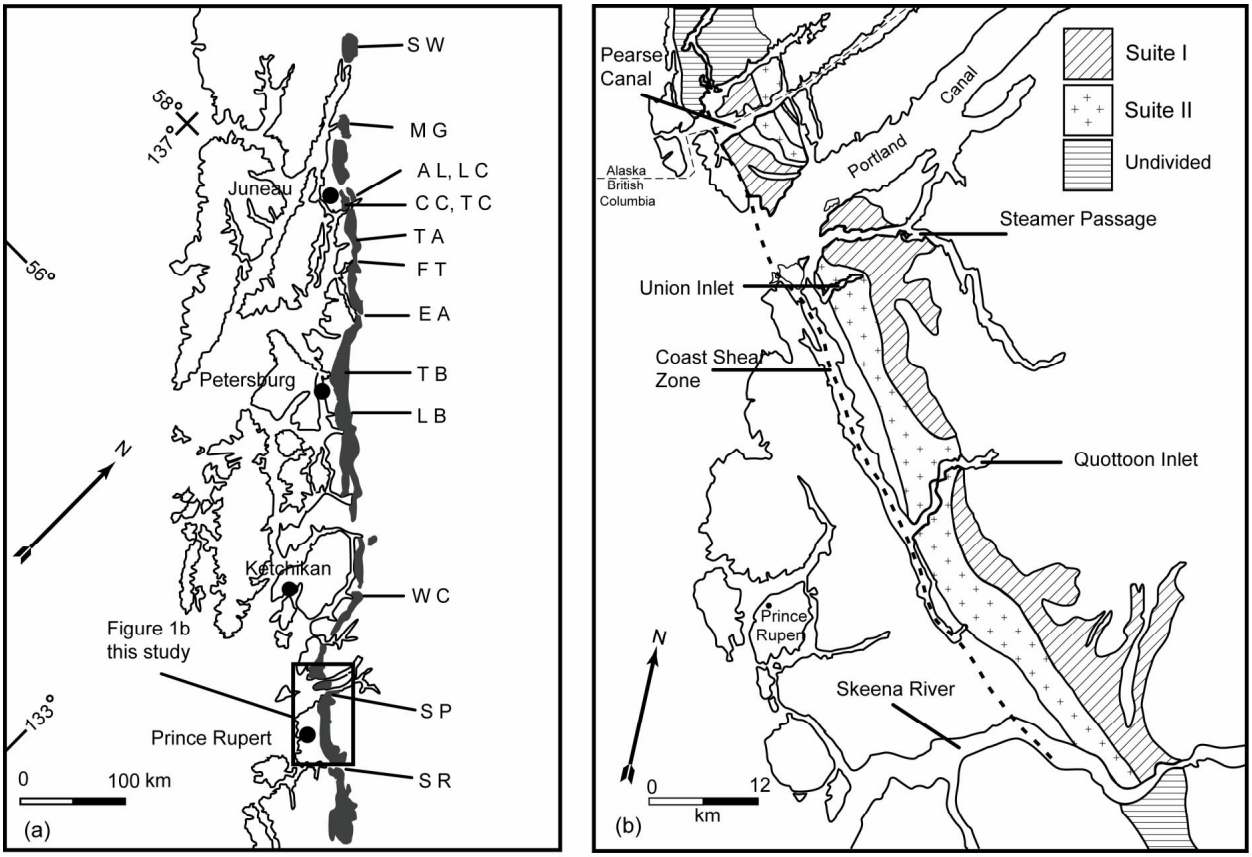

Figure 1. Location maps showing (a) the area of this study (outlined in the box) with respect to the Great Tonalite Sill and locations with available geochemical, isotopic, and/or geochronologic data, and (b) the location of suites I and II of the Quottoon Igneous Complex along the five transects discussed in this study. Abbreviations are as follows: SW=tonalite NW of Skagway, MG=Mendenhall Glacier pluton, AL=Annex Lakes pluton, LC=Lemon Creek pluton, CC=Carlson Creek pluton, TC=Taku Cabin pluton, TA=tonalite at Tracy Arm, FT=tonalite at Tracy Arm, EA=tonalite at Endicott Arm, TB=tonalite at Thomas Bay, LB=tonalite at LeConte Bay, WC=tonalite at Walker Cove, SP=Quottoon pluton along Steamer Passage, SR=Quottoon pluton along the Skeena River. Data sources are Arth et al. (1988), Drinkwater et al. (1989, 1990), The Quottoon Pluton is one of many plutons of the Great Tonalite Sill that represent a significant peak in magmatism spanning the latest Cretaceous through Eocene times (fig. 1a) (Armstrong, 1988; Gehrels et al., 1991; Woodsworth, 1992; Brew, 1994). Structural analysis of many plutons throughout the Great Tonalite Sill confirmed previous suggestions that some bodies were of a composite nature (Hollister, et al., 1987, Drinkwater et al.,1989, 1990, 1995; Gehrels et al., 1991; Ingram, 1992). However, the origin and magmatic evolution of most plutons of the Great Tonalite Sill is not well understood. It remains unclear whether the composite plutons are the result of distinct magmas emplaced in close spatial association or magmas related to each other through petrologic processes (e. g. fractional crystallization)

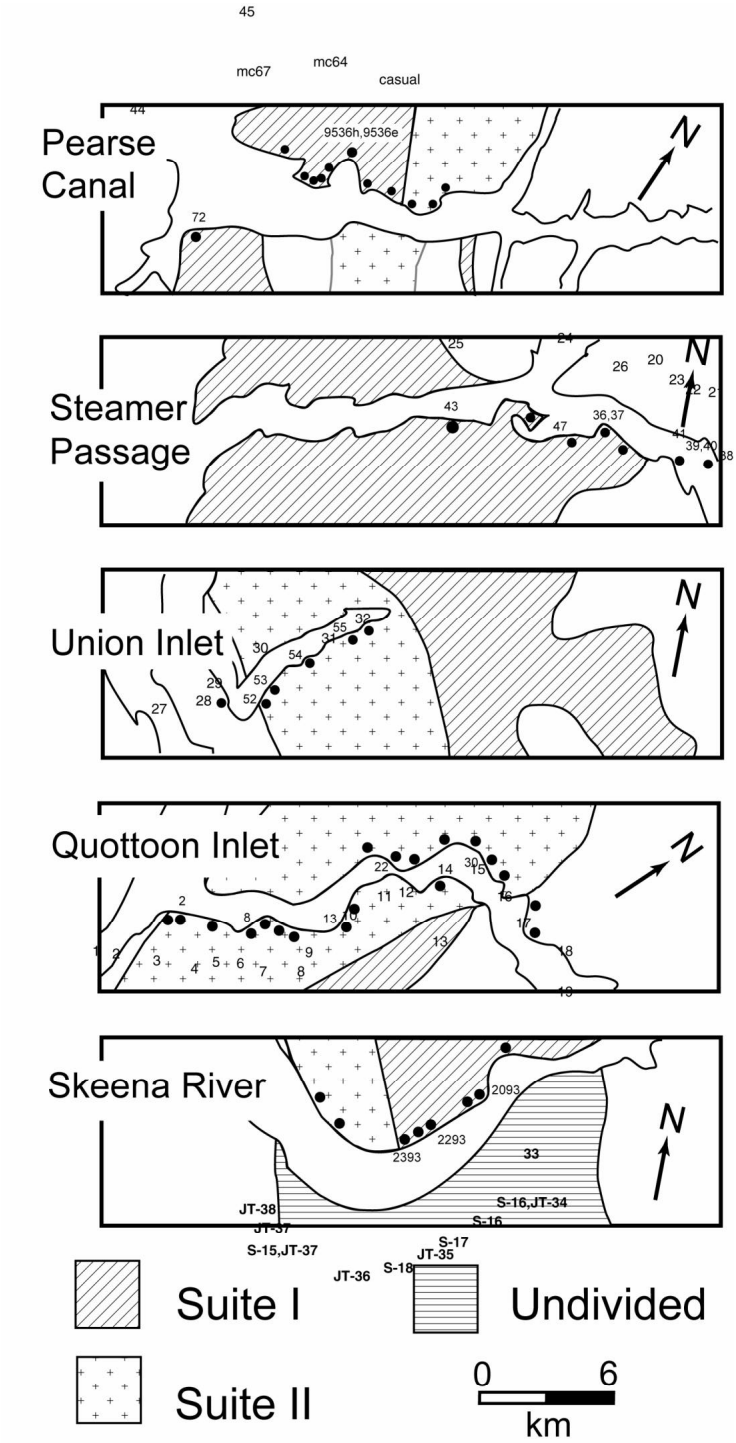

Figure 2. Maps for the individual transects across the QIC showing the sample numbers and locations as solid circles. Also shown are the locations where field data was collected but no sample was analyzed for geochemistry (locations without sample numbers). Map patterns are the same as in figure 1. Most of the western contact is in close proximity to the CSZ (<3km) except near the Skeena River where it is ~5 km from the CSZ. Field observations along five traverses from the Skeena River to Pearse Canal (fig. 1b and 2) suggest that there are mappable differences in color indices, association of mafic enclaves and dikes, deformation style, and degree of wall rock involvement amongst individual traverses and result in our defining two distinct igneous suites.

Field Relations

In the study area the QIC is ~ 100 km long and always less than 15 km wide stretching from Pearse Canal to the Skeena River (fig. 1b). The rocks are quartz dioritic in composition and intrude the upper amphibolite facies gneisses of the Central Gneiss Complex. (Hutchison, 1982; Hollister, 1982; Crawford and Hollister, 1983; Crawford et al., 1987).

The suite I rocks are lithologically heterogeneous ranging from diorites (Steamer Passage and Pearse Canal) to strongly foliated quartz diorites (Steamer Passage and Skeena River) to mafic quartz diorites with abundant mafic enclaves (Steamer Passage and Pearse Canal) as well as felsic quartz diorites with abundant rusty metasedimentary xenoliths and screens (e. g. Skeena River and Pearse Canal). The origin of the mafic enclaves and dikes is uncertain, but the xenoliths and screens appear similar to the rusty metasedimentary wall rocks of the Central Gneiss Complex. Well-developed hornblende-biotite foliations, grain size reduction, and elongate enclaves (x:z > 10) document the strongly deformed nature of the suite I rocks. It is likely that such fabric styles developed in the solid state (Patterson et al., 1989, Ingram, 1992). The interaction of mafic enclaves and dikes with the quartz diorites likely resulted in the heterogeneous nature of rocks within suite I.

In contrast, the suite II quartz diorites are undeformed, contain primary magmatic features, do not contain abundant metasedimentary xenoliths or screens, have equidimensional textures (e. g. plagioclase and hornblende of 1.5 cm), and are coarser-grained than the rocks of suite I. Suite II rocks are located along Quottoon Inlet and Union Inlet. Suite II rocks are homogeneous throughout, contain flow aligned plagioclase and melt filled shears indicative of deformation in the presence of melt (Patterson et al., 1989, Ingram, 1992). The rocks along central portions of Quottoon Inlet and Union Inlet are altogether unfoliated. Mafic enclaves and dikes are present in suite II but occur in discrete areas. The absence of solid-state deformational features and lack of mafic enclaves provide a means for identification of suite II rocks in the field.

Mafic dikes are fine-grained and range from 10 cm to 2 m in width and are randomly oriented and distributed. The mafic dikes are especially abundant along the Steamer Passage and Pearse Canal transects, although, one large (>100 m wide) appinitc dike was noted along the Skeena River transect. Some mafic dikes in suite I are disaggregated into swarms of enclaves

that are commonly 10 cm to 1 m along the longest dimension (x:z). Mafic enclaves are parallel to foliation in deformed rocks, while they are randomly oriented in undeformed rocks. Also, some mafic dikes and enclaves occur only as "ghosts" due to extensive interaction with surrounding quartz diorite, while others have sharp boundaries suggesting rapid chilling and limited interaction with the host magma. Plagioclase, biotite, and amphibole comprise the mafic enclave and dike mineralogy.

Petrography and Mineral Chemistry

The majority of the samples from both suites I and II plot within the quartz diorite field of Strekeisen (1973) (table 1). The two suites exhibit minor differences in modal abundance of alkali feldspar which is generally more abundant in suite I. The quartz diorites of suite I have a wide range of color indices (24-50) and variable hornblende:biotite ratios (0.2 to 5.3) that do not correlate with geographic location or color index (table 1). In suite II the color indices and hornblende:biotite ratios (24-34 and 0.28 to 1.59 respectively) do not vary as much as those in suite I (table 1). Textural relationships indicate that both suites have similar sequences of crystallization with early crystallizing opaque minerals (magnetite and ilmenite), zircon and sphene followed by apatite, hornblende, biotite, and plagioclase. Quartz and potassium feldspar are the latest crystallizing phases. Additional petrographic information and mineral chemistry is available in Kenah (1979).

The hornblende (0.3 cm to 1.5 cm) has brownish green to bluish-green pleochroism and is always subhedral (rare) to anhedral. Most hornblende crystals have sieve textures, and their grain boundaries are very irregular apparently due to interaction with residual magma. A crystallization pressure of 4.6 kb ($\pm$0.6 kb) is inferred (sample 20 in fig. 2) using the Al in hornblende barometer (Schmidt, 1992). The analyzed sample has the requisite mineral assemblage and the hornblende rims were analyzed. These pressures agree closely to those determined from wall rock geobarometers of 4.6 + 0.5 kb Kenah, 1979).

Biotite (0.5 cm) occurs as euhedral laths that have strong pleochroism from brown to reddish-brown. In rocks associated with abundant mafic enclaves and dikes, the biotite often forms net-shaped framework clusters separated by highly reacted hornblende. Biotite crystals enclosed in hornblende are commonly surrounded by opaque oxide inclusions and are interpreted to be a

result of decreased hornblende stability during magma evolution as the water content of the magma increases favoring biotite stability (Naney, 1983). The biotite Mg/(Mg + Fe) ranges from 0.508 to 0.534 and plot on the phlogopite-biotite join where Mg:Fe is ~2:1.

Plagioclase ranges from anhedral fine-grained (0.1 cm) to tabular and coarse-grained (1.5 cm). Fine-grained plagioclase (through grain-size reduction), bent twin lamellae, and subgrain formation are common in rocks that have undergone solid-state deformation. In contrast, flow aligned plagioclase is common in rocks that underwent deformation in the magmatic state (see Patterson et al., 1989; Ingram, 1991). Sericite and saussurite, are only minor constituents in plagioclase and occur as late stage alteration products. Plagioclase feldspars range in composition from An_{28} to An_{34}.

Quartz (0.5 cm) is strained (undulose extinction/subgrain formation) in deformed rocks near the contacts suggesting solid-state deformation in these areas. In relatively undeformed rocks, it commonly occurs as equidimensional, interstitial aggregates.

Alkali feldspar (0.5 cm) is rare to absent in the rocks of the QIC. When present, it is always sub- to anhedral. It usually occurs as a late crystallizing phase that is interstitial to a variety of minerals. It is commonly altered to sericite and saussurite. The potassium feldspar composition is $Or_{86\text{-}88}$.

A variety of accessory minerals are present in trace amounts (< 2 %). Opaque minerals (ilmenite and magnetite) are <0.3 cm across and range from anhedral to cubic. Ilmenite possesses a wide range of compositions from Il_{25} to Il_{89}. Ilmenite commonly occurs as rims around anhedral sphene. The magnetite has composition of $Mag_{98}Chr_1Usp_{0.6}Gax_{0.4}$. Anhedral to euhedral sphene crystals (up to 0.7 cm) are common and are associated with clusters of biotite and hornblende. Apatite is ubiquitous in all samples and ranges from stubby (length/width ratio of 2) to acicular (length/width ratio of 10). It has a long crystallization interval and it is most commonly enclosed in plagioclase. Zircons are typically clear and euhedral prisms with length/width ratios of 5 and occur most commonly as inclusions in biotite. Rarely, they occur as brown crystals with opaque inclusions.

Table 1. Percent modal mineral abundances for samples from the QIC. 600 points were counted for each thin section.

	Suite I										
sample #	**36**	**39**	**40**	**41**	**43**	**47**	**72**	**2093**	**2293**	**2393**	**536h**
rock type	QD	QD	D	QD	QD	QD	QD	QD	QD	QD	QD
plagioclase	62	62	57	43	59	60	62	66	67	60	58
biotite	16	28	22	16	13	21	10	17	16	12	6
hornblende	13	5	14	33	17	11	18	9	11	22	31
K-feldspar	2	1	2	3	3	1	tr	tr	n.d.	tr	1
quartz	6	4	3	5	8	6	10	8	6	6	4
apatite	tr	tr	tr	tr	tr	2	tr	tr	tr	tr.	tr
sphene	tr	tr	tr	tr	tr	tr	tr	n.d.	tr	tr	tr
opaques	1	tr	tr	1	1	tr	tr	tr	tr	tr.	tr
zircon	tr	tr	tr	tr	tr	tr	tr	tr	tr	tr.	tr
chlorite	n.d.	n.d.	n.d.	n.d.	n.d.	n.d.	n.d.	tr	tr	n.d.	n.d.
epidote	tr	tr	n.d.	n.d.	n.d.	n.d.	tr	tr	n.d.	tr	n.d.
sericite	tr	n.d.	tr	tr	tr	n.d.	tr	tr	n.d.	n.d.	n.d.
hb:bi	0.8	0.2	0.6	2.1	1.3	0.5	1.8	0.5	0.7	1.9	5.3
color index	30	34	37	50	31	34	28	25	27	34	37

Table 1. continued.

	Suite II									Enclaves		Dikes	
sample #	**2**	**8**	**13**	**22**	**30**	**52**	**53**	**54**	**55**	**536e**	**37**	**17**	**44**
rock type	QD	QD	QD	QD	QD	QD	QD	QD	QD	D	D	D	D
plagioclase	63	64	63	62	69	59	56	60	69	40	42	64	54
biotite	11	15	23	19	19	13	15	15	10	20	19	21	17
hornblende	14	12	7	12	8	20	18	17	13	38	34	10	23
K-feldspar	1	1	2	tr	1	n.d.	1	1	tr	tr	n.d.	tr	3
quartz	10	8	4	5	2	7	9	6	7	tr	2	1	1
apatite	tr	tr	tr	tr	tr	tr	tr	1	tr	tr	1	1	tr
sphene	tr	tr	1	tr	tr	1	tr	tr	tr	tr	1	2	2
opaques	tr.	tr	tr	tr	tr	tr	tr	tr	1	tr	1	1	tr
zircon	tr	tr	tr	tr	tr	tr	tr	tr	tr	tr	tr	tr	tr
chlorite	tr	tr	tr	n.d.	n.d.	n.d.	n.d.	n.d.	n.d.	n.d.	n.d.	n.d.	n.d.
epidote	tr	1	tr	n.d.	tr	tr	tr	n.d.	tr	n.d.	tr	tr	n.d.
sericite	tr	tr	tr	n.d.	tr	n.d.	n.d.	n.d.	n.d.	n.d.	tr	n.d.	tr
hb:bi	1.3	0.8	0.3	0.6	0.4	1.6	1.2	1.2	1.3	1.9	1.8	0.5	1.4
color index	28	26	31	32	27	34	34	33	24	60	56	35	43

Notes: QD=quartz diorite; D=diorite. tr., volume of mineral <1%. n.d., mineral not detected. 536h is the proximal host to the mafic enclave 536e.

Secondary phases are chlorite, sericite, myrmekite, and epidote which always occupy <1 modal percent of rocks.

The main petrographic features that distinguish the suite I rocks from those of suite II are the variable hornblend:biotite ratios (0.8-5.31) and the highly variable color indices (27-50; table 1) demonstrating the heterogeneous nature of the suite I rocks. Suite I rocks have well developed biotite-hornblende foliations, crenulate grain boundaries, a lack of euhedral minerals, and strained quartz crystals. Mineral textures range from anhedral to hypidiomorphic. Grain sizes are highly variable ranging from fine- to coarse-grained. Some fine-grained rocks are the result of interaction with mafic enclaves and dikes, whereas, others are the result of deformation. Abundant microstructures document the importance of solid-state deformation throughout suite I. In all rocks, plagioclase and quartz subgrain formation demonstrates grain size reduction. The quartz in gneissic rocks of suite I has a slight ribbon shape suggestive of high temperature deformation.

In comparison to the suite I rocks, the rocks from suite II are more homogeneous. Minerals in suite II are equidimensional and do not show structural evidence of extensive solid state deformation (i. e. plagioclase subgrain formation). Only locally do the suite II rocks record solid state deformation (e. g. near the contacts). A variety of primary magmatic textures range from flow alignment of minerals to random mineral orientation developed in a static crystallization environment. Also, some meter scale shears are filled with melt. Such features and mineral textures suggest that some portions of suite II encountered deformation during the presence of melt while other portions sustained no deformation.

Mafic dikes and enclaves from both suites are diorites (Strekeisen, 1973). The mineralogy and sequence of crystallization of mafic enclaves and dikes are similar to the host quartz diorites except that they have higher percentages of mafic silicates (table 1). Enclaves and dikes are fine- and even-grained (~1 mm) and have a wide range of color indices (34-88) (table 1). The hornblende in enclaves (1-5 mm) is highly reacted. Relict hornblende occurs in reaction relations with clusters of greenish-brown to reddish-brown colored groundmass biotite, sphene, opaque oxides, and fine-grained plagioclase. These features are accentuated in the “ghosted enclaves”. Porphyritic enclaves are mineralogically similar to the fine- and even grained mafic enclaves/dikes except they have large crystals (~1 cm) of plagioclase, biotite, and hornblende set in a groundmass of biotite, hornblende, and plagioclase. The plagioclase in the porphyritic

enclaves is commonly zoned. Minor quartz (~0.2 cm) is strained and has well-developed subgrains and undulose extinction. Igneous textures such as zoned plagioclase and flow aligned phenocrysts in the enclaves suggest that they crystallized from a melt (Vernon, 1983). No refractory restitic minerals such as garnet or pyroxene are present in any of the analyzed mafic enclaves or dikes.

Whole Rock and Sr Isotope Geochemistry

Twenty-five samples from five transects across the QIC (see fig. 2 for sample locations) were selected for major, trace, rare earth element (REE), and Sr isotopic analyses. Table 2 lists the major and trace element contents, table 3 shows the REE concentrations, and table 4 lists the initial $^{87}Sr/^{86}Sr$ ratios (Sr_i). Twenty-two samples are quartz diorites, two are dioritic mafic enclaves, and two are dioritic mafic dikes (table 1). One enclave was analyzed along with its proximal host quartz diorite (536e and 536h).

The QIC quartz diorites define a calc-alkaline trend on traditional AFM diagrams; more mafic suite I rocks, enclaves, and dikes are mildly enriched in iron. None of the QIC rocks have aluminum saturation indices (A/CNK) <1.0 (table 2).

In suite I, the Sr_i ranges from 0.70512 to 0.70717 (fig. 6a and table 4). No simple correlation exists when plotted against silica; however, several important features are apparent. There is considerable variation in Sr_i, which varies from 0.70553 to 0.70672 over a small silica range of ~1 wt. % in the most mafic rocks. The higher-silica rocks have a range in Sr_i values from 0.70513 to 0.70717. The enclaves plot over a similar Sr_i range as the silica-poor rocks from suite I (0.70585-0.70660).

Table 2. Major and trace element abundances for the Quottoon Igneous Complex

	Suite I										
Sample #	**36**	**39**	**40**	**41**	**43**	**47**	**72**	**2093**	**2293**	**2393**	**536h**
SiO_2 (wt.%)	53.71	62.69	53.65	53.59	56.11	63.06	62.39	62.31	60.26	58.99	54.85
TiO_2	1.26	0.87	1.42	1.23	0.90	0.76	0.70	0.72	0.83	0.85	0.85
Al_2O_3	17.75	17.00	18.30	15.86	18.52	17.28	16.25	16.16	16.85	16.87	18.15
FeO_t	8.73	5.27	9.15	9.70	6.98	5.33	5.73	5.18	5.74	6.60	8.64
MnO	0.13	0.07	0.13	0.15	0.09	0.08	0.10	0.10	0.11	0.12	0.15
MgO	4.13	1.85	3.76	5.77	3.41	2.39	2.54	2.96	2.90	3.74	3.74
CaO	6.98	4.88	6.61	7.89	6.84	5.39	5.23	4.89	5.68	6.30	8.52
Na_2O	3.75	3.98	3.75	2.99	4.07	4.20	3.54	3.97	3.99	3.87	4.01
K_2O	2.00	1.76	2.33	1.44	1.53	1.78	2.08	2.25	1.59	1.87	1.19
P_2O_5	0.43	0.27	0.43	0.44	0.60	0.27	0.22	0.18	0.21	0.20	0.22
total	98.87	98.64	99.53	99.06	99.05	100.54	98.78	98.72	98.16	99.41	100.32
LOI	0.67	0.35	0.5	0.55	0.51	0.34	0.37	0.65	1.55	0.80	0.41
A/CNK	0.84	0.98	0.88	0.76	0.89	0.93	0.92	0.91	0.91	0.85	0.78
Rb (ppm)	54	49	57	38	32	51	69	48	36	51	20
Sr	725	636	640	549	1135	687	642	649	545	608	742
Ba	1295	1120	1328	987	1096	1368	1128	n.a.	n.a.	n.a.	603
Zr	235	216	148	72	138	160	90	130	109	116	253
Y	26	16	20	23	14	17	17	14	21	22	33
Hf	6	4	4	2	4	4	3	n.a.	n.a.	n.a.	7
Nb	15	9	19	13	8	11	10	6	8	6	13

Table 2. continued.

	Suite II									Enclaves		Dikes	
Sample #	**2**	**8**	**13**	**22**	**30**	**52**	**53**	**54**	**55**	**536e**	**37**	**17**	**44**
SiO_2 (wt.%)	60.44	58.63	59.87	62.34	60.33	60.62	58.03	58.53	56.80	50.31	47.32	48.68	50.84
TiO_2	0.73	0.92	0.99	0.70	0.78	0.79	0.83	1.15	0.94	1.37	1.52	1.37	1.61
Al_2O_3	17.12	16.69	17.05	16.91	17.18	17.01	18.46	16.60	18.86	17.98	19.19	20.41	20.44
FeOt	5.64	6.91	6.26	5.38	5.88	5.79	5.95	7.15	6.67	10.52	11.30	10.46	8.56
MnO	0.08	0.13	0.09	0.08	0.10	0.09	0.08	0.10	0.09	0.17	0.17	0.14	0.11
MgO	2.67	3.38	2.80	2.41	2.79	3.25	2.93	3.50	3.20	4.72	5.40	3.76	3.59
CaO	5.25	5.87	5.69	5.02	5.60	5.86	6.64	6.72	6.82	8.10	8.76	8.94	7.98
Na2O	3.71	3.68	4.19	4.00	4.01	3.74	4.22	3.54	4.21	3.58	3.28	4.20	4.49
K_2O	2.70	1.84	1.75	2.49	1.77	1.98	1.69	1.76	1.50	2.09	2.39	1.50	1.58
P_2O_5	0.22	0.26	0.32	0.24	0.24	0.23	0.27	0.30	0.30	0.36	0.41	0.55	0.54
total	98.56	98.31	99.01	99.57	98.68	99.36	99.10	99.35	99.39	99.20	99.74	100	99.74
LOI	0.51	0.61	0.43	0.35	0.56	0.36	0.42	0.60	0.39	0.45	0.76	0.35	0.57
A/CNK	0.92	0.89	0.89	0.92	0.92	0.9	0.89	0.83	0.9	0.79	0.8	0.82	0.87
Rb (ppm)	54	45	40	64	39	42	37	37	32	59	58	23	36
Sr	911	944	1079	782	926	847	1142	931	1116	693	618	1448	1338
Ba	2245	1197	1195	1189	1191	1107	1154	1102	1146	1437	1264	940	1466
Zr	154	142	176	144	105	109	138	233	107	215	96	134	168
Y	11	16	12	12	10	10	12	21	11	32	31	19	15
Hf	4	4	5	4	3	3	4	6	3	6	3	3	4
Nb	8	9	10	11	9	8	8	14	7	16	9	10	14

Note: n. a., element not analyzed. n.d., element not detected. 536h is the proximal host to the mafic enclave 536e.

Table 3. Rare earth element abundances for samples from the QIC.

	Suite I										
Sample #	**36I**	**39I**	**40I**	**41I**	**43I**	**47I**	**72I**	**2093I**	**2293I**	**2393I**	**9536 h**
La (ppm)	38.2	25.9	31.6	23.7	20.3	30	19.2	22	22.2	21	20.7
Ce	73.4	48.8	61.3	49.1	41.6	52.9	40.0	44	46	44	57.3
Nd	32.5	21.1	27.6	24.4	19.7	22.3	18.9	20	20	19	35.9
Sm	6.8	4.2	5.5	5.3	4.2	4.6	4	4	4.1	4.2	8.2
Eu	1.7	1.6	1.8	1.5	1.3	1.3	1.4	1.1	1.1	1.2	1.9
Gd	5.8	5	4.8	5	3.6	3.9	4.2	n. a.	n. a.	n. a.	8.1
Tb	0.8	0.6	0.6	0.7	0.5	0.5	0.6	0.4	0.5	0.5	1.1
Dy	4.5	2.8	3.6	4	2.5	3.0	2.8	n. a.	n. a.	n. a.	5.7
Ho	0.9	n.d.	0.7	0.8	0.5	0.6	n.d.	n. a.	n. a.	n. a.	n.d.
Er	2.6	1.5	2.0	2.3	1.3	1.7	1.6	n. a.	n. a.	n. a.	3.2
Tm	0.33	0.2	0.3	0.3	0.2	0.2	0.2	n. a.	n. a.	n. a.	0.4
Yb	2.1	1.2	1.8	2.0	1	1.4	1.5	1.2	1.9	2.1	2.7
Lu	0.34	0.2	0.3	0.3	0.2	0.2	0.2	0.2	0.3	0.3	0.4
Eu/Eu*	0.84	1.0	1.1	0.9	1.0	1.0	1.0	-	-	-	0.7
La_N/Yb_N	12.2	14.4	11.7	7.9	13.6	14.3	8.6	12.2	7.7	6.8	5.1

Table 3. continued.

	Suite II									Enclaves		Dikes	
Sample #	**2**	**8II**	**13II**	**22II**	**30II**	**52II**	**53II**	**54II**	**55II**	**37 e**	**9536 e**	**17 d**	**44 d**
La (ppm)	22.2	47.9	26.4	36.7	25.9	28.2	53.0	25.2	33.3	19.3	25.8	22.0	23.8
Ce	40.1	91.0	53.0	64.2	45.9	51.9	86.6	60.9	57.3	43.5	66.3	51.2	53.0
Nd	17.7	33.9	23.5	23.9	18.4	19.3	27.2	31.9	21.8	24.7	39.0	28.4	26.4
Sm	3.6	6.1	4.6	4.1	3.4	3.5	4.4	6.8	3.9	6.2	8.6	6.2	5.5
Eu	1.2	1.5	1.4	1.1	1.1	1.0	1.3	2.2	1.2	1.8	2.2	1.9	1.6
Gd	3.1	4.7	3.7	3.5	3.0	3.0	3.4	5.4	3.3	5.7	8.2	5.1	4.4
Tb	0.4	0.6	0.4	0.5	0.4	0.4	0.4	0.7	0.4	0.8	1.2	0.7	0.6
Dy	2.2	3.0	2.3	2.3	1.9	1.8	2.2	3.7	2.0	5.2	5.7	3.6	2.6
Ho	0.4	0.6	0.4	0.4	0.4	0.3	0.4	0.7	0.4	0	0	0.6	0.5
Er	1.1	1.6	1.1	1.2	1.0	1.0	1.2	1.9	1.1	3.2	3.3	1.9	1.3
Tm	0.12	0.2	0.1	0.2	0.1	0.1	0.1	0.2	0.1	0.4	0.4	0.2	0.2
Yb	0.8	1.2	0.8	1.0	0.8	0.8	1.0	1.6	0.9	2.6	2.7	1.4	1.2
Lu	0.12	0.2	0.1	0.2	0.1	0.1	0.2	0.3	0.1	0.4	0.4	0.2	0.2
Eu/Eu*	1.1	0.8	1.1	0.9	1.1	0.9	1.1	1.1	1.1	0.9	0.8	1.0	1.0
La_N/Yb_N	18.5	26.0	22.1	24.5	21.7	23.6	35.4	10.5	24.7	5.0	6.4	10.5	13.3

Note: abbreviations same as in table 2.

Table 4. Sr isotopic data for the Quottoon Igneous Complex.

	Sample #	Rb (ppm)	Sr (ppm)	$^{87}Sr/^{86}Sr_m$	$^{87}Sr/^{86}Sr_i$
Suite I	36	54	725	0.70581(8)	0.70563
	39	49	636	0.70572(2)	0.70553
	40	57	640	0.70642(8)	0.70620
	41	38	549	0.70622(4)	0.70605
	47	51	687	0.70583(10)	0.70565
	72	69	642	0.70743(7)	0.70717
	2093	48	649	0.70650(11)	0.70632
	2293	36	545	0.70529(5)	0.70513
	2393	51	608	0.70554(8)	0.70528
	9536 h	20	742	0.70678(7)	0.70672
Suite II	2	54	911	0.70691(5)	0.70677
	8	45	944	0.70622(10)	0.70618
	13	40	1079	0.706319(5)	0.70623
	22	64	782	0.70706(21)	0.70686
	52	42	847	0.70698(3)	0.70659
	53	37	1142	0.70647(11)	0.70639
	54	37	931	0.70627(10)	0.70617
	55	32	1116	0.70638(4)	0.70631
Mafic Enclaves	37e	57	618	0.70607(8)	0.70585
	9536 e	59	693	0.70681(7)	0.70660
Central Gneiss Complex	1593	63	475	0.70602(7)	0.70526
	893	27	285	0.70525(6)	0.70506
	1293	50	1056	0.70470(14)	0.70459
	38	61	440	0.70610(8)	0.70530
	GMO	21	369	0.70496(3)	0.70464

Notes: $^{87}Sr/^{86}Sr_m$, measured ratio; $^{87}Sr/^{86}Sr_i$ initial ratios are age corrected to 58.6 Ma; Numbers in parentheses are $\pm$ two standard errors of the mean ($\pm 2\sigma_m$);Central Gneiss samples: 1593, garnet gneiss; 893, felsic gneiss; metatonalite; 38, rusty metasediment; GMO, garnet sillimanite gneiss (provided by Lincoln Hollister).

Suite I

The quartz dioritc rocks from suite I have a silica range from 53.6 to 63.1 wt. % (fig. 3) where silica concentrations do not correlate with geographic location. All samples from suite I show large variations amongst all major elements at constant silica. FeO_t, MgO and CaO display the most linear and coherent trends over the entire range of silica concentration. K_2O displays a break in the trend line at 56 wt. % SiO_2; the low-silica rocks have a strong negative trend with increasing SiO_2 while the higher-silica rocks define a positive trend. Considerable variation in TiO_2, Al_2O_3, MgO, CaO, and K_2O exists at any given silica concentration illustrating the heterogeneous nature of rocks from suite I.

Large variations also exist amongst the large ion lithophile elements (LILE) and the high field strength elements (HFSE) in the suite I rocks. The low-silica rocks show a strong negative correlation in Rb concentration when plotted against SiO_2; whereas, in the higher-silica rocks Rb shows a positive correlation with SiO_2 (fig. 3). Rb concentration decreases by 40 ppm between 54 and 56 wt. % SiO_2 in the low-silica series rocks and increases from 31.7 ppm to 69 ppm over a SiO_2 range of ~6 wt. % in the higher-silica rocks. Sr concentrations range from 549 to 742 ppm and define a shallow trend over the entire silica interval (fig. 3). The low silica rocks show considerable variation in Ba at constant silica (603 to 1328 ppm). On MORB (mid-ocean ridge basalt) normalized diagrams the suite I rocks have similar elemental abundances as the suite II rocks but are more enriched in HFSE (fig. 4). The rocks show high LILE:HFSE ratios ($Ba_N/Y_N \approx 20$) typically attributed to a subduction-related origin (Hawkesworth et al., 1994; Pearce and Peate, 1995).

Suite I rocks have shallow rare earth element patterns (average La_N/Yb_N=11.4) and smooth trends that do not show significant anomalies (fig. 5, table 3). Small negative Eu anomalies (Eu/Eu* = 0.7 and 0.8) are developed in only two samples (table 4). The REE abundances for suite I samples have a larger range and notably lower La_N/Yb_N ratios than in suite II (see below).

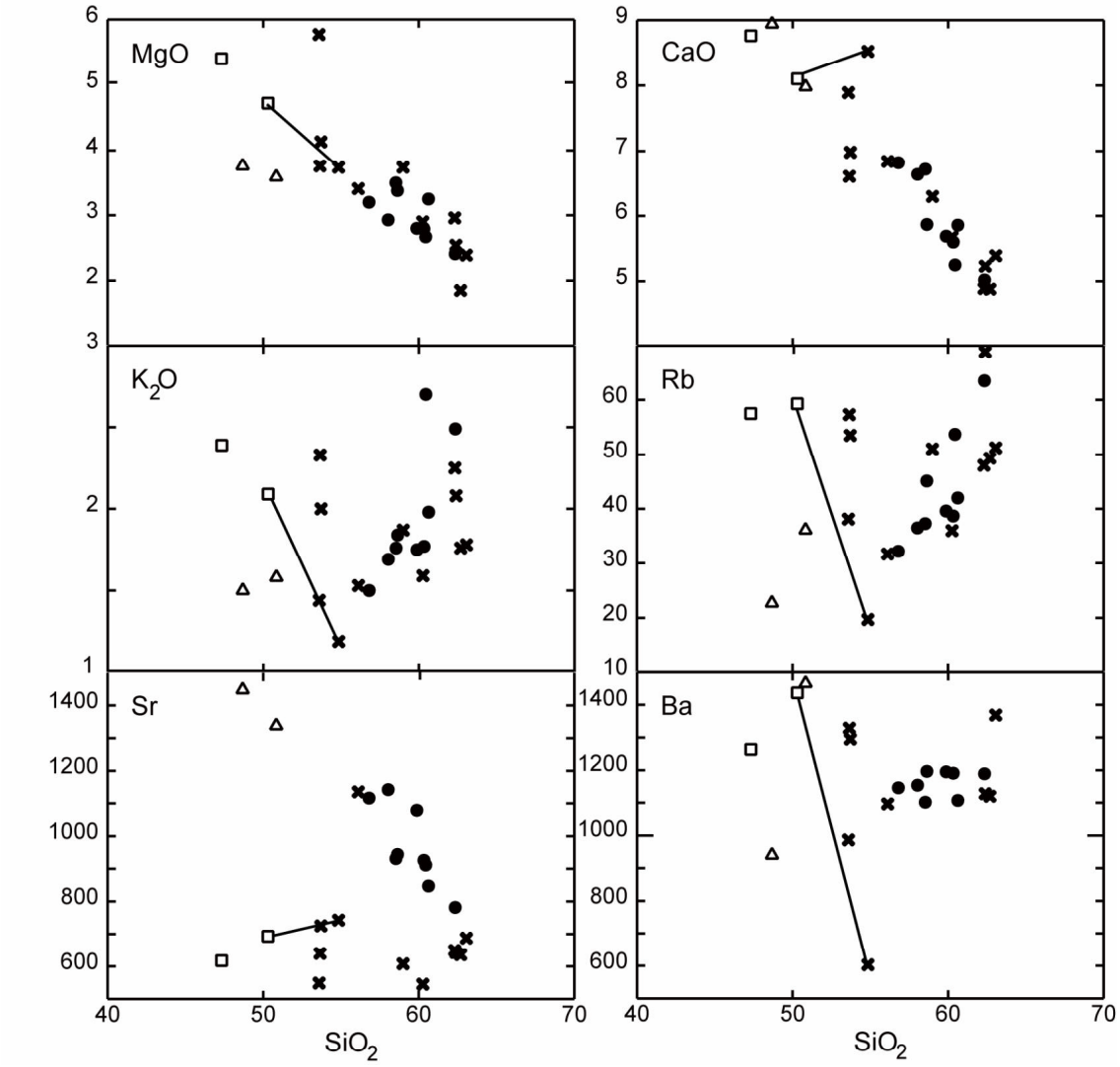

Figure 3. Harker diagrams for representative major and trace elements (in weight %) from the Quottoon Igneous Complex. The line connects an enclave host pair. Symbols are as follows: x's=suite I, solid circles=suite II, open squares=mafic enclaves, open triangles=mafic dikes.

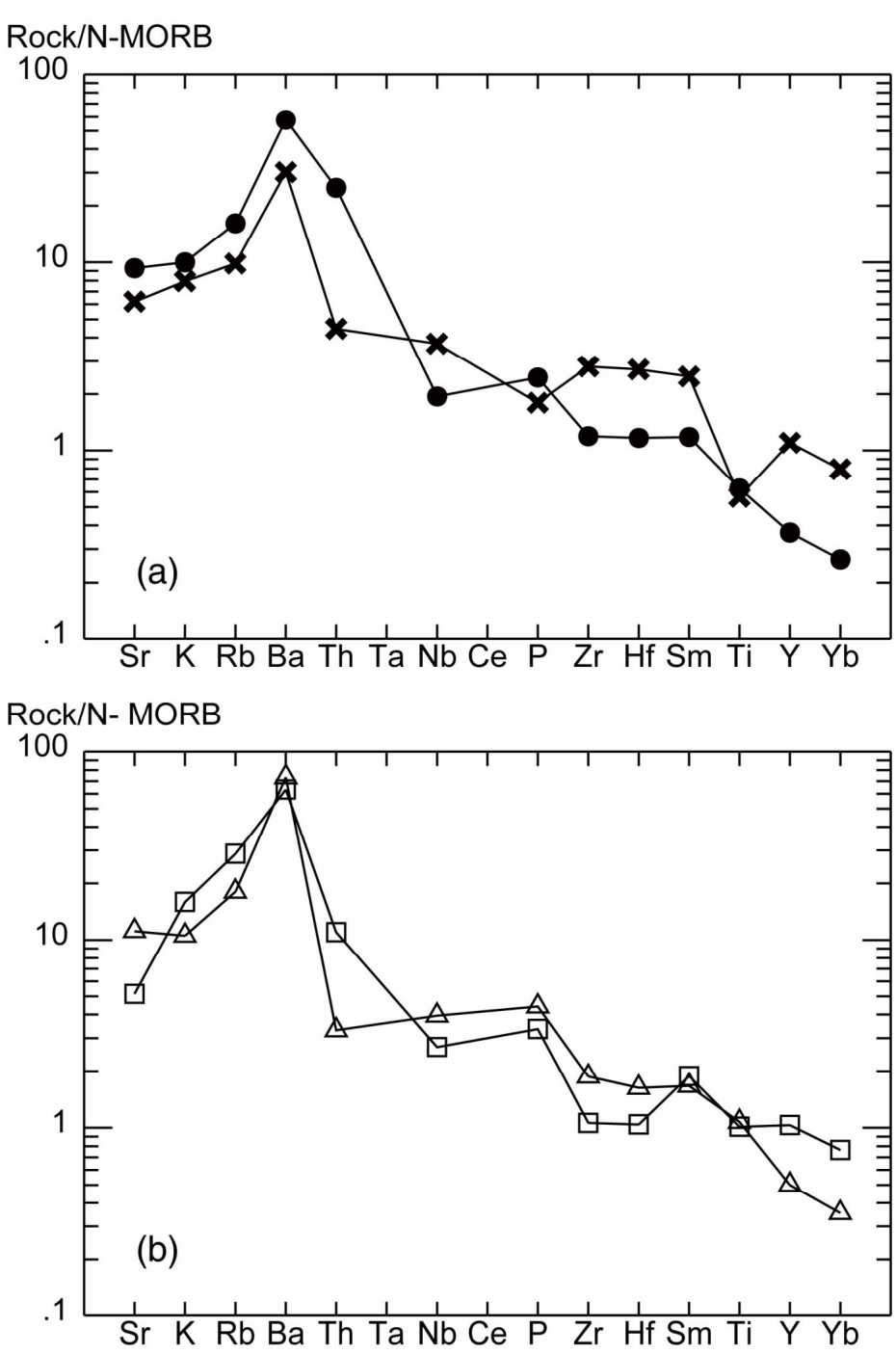

Figure 4. N-MORB normalized trace element abundance patterns (Saunders and Tarney, 1984) for moderately to highly incompatible elements shown for representative samples of (a) suite I and II (samples 536b and 55 respectively), and (b) enclaves and dikes (samples 37 and 44 respectively). Symbols are the same as in figure 3.

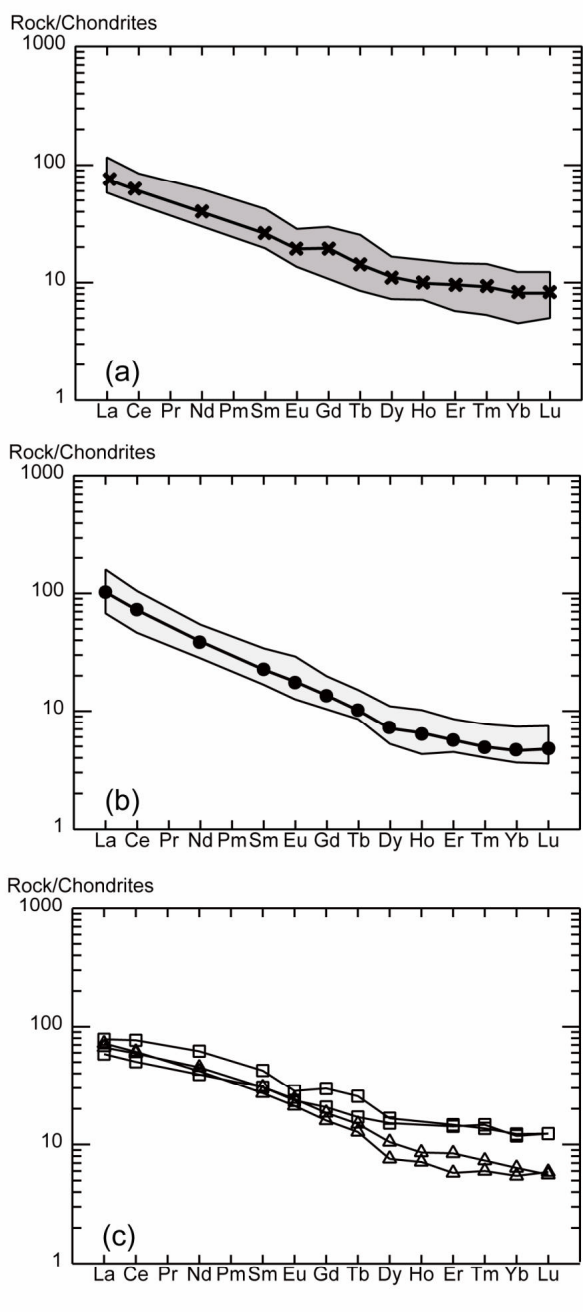

Figure 5. Chondrite normalized rare earth element patterns (Nakamura, 1974) for (a) suite I, (b) suite II, and (c) enclaves and dikes. The shaded region shows the range of abundances and the lines connect the averages. Symbols are the same as in figure 3.

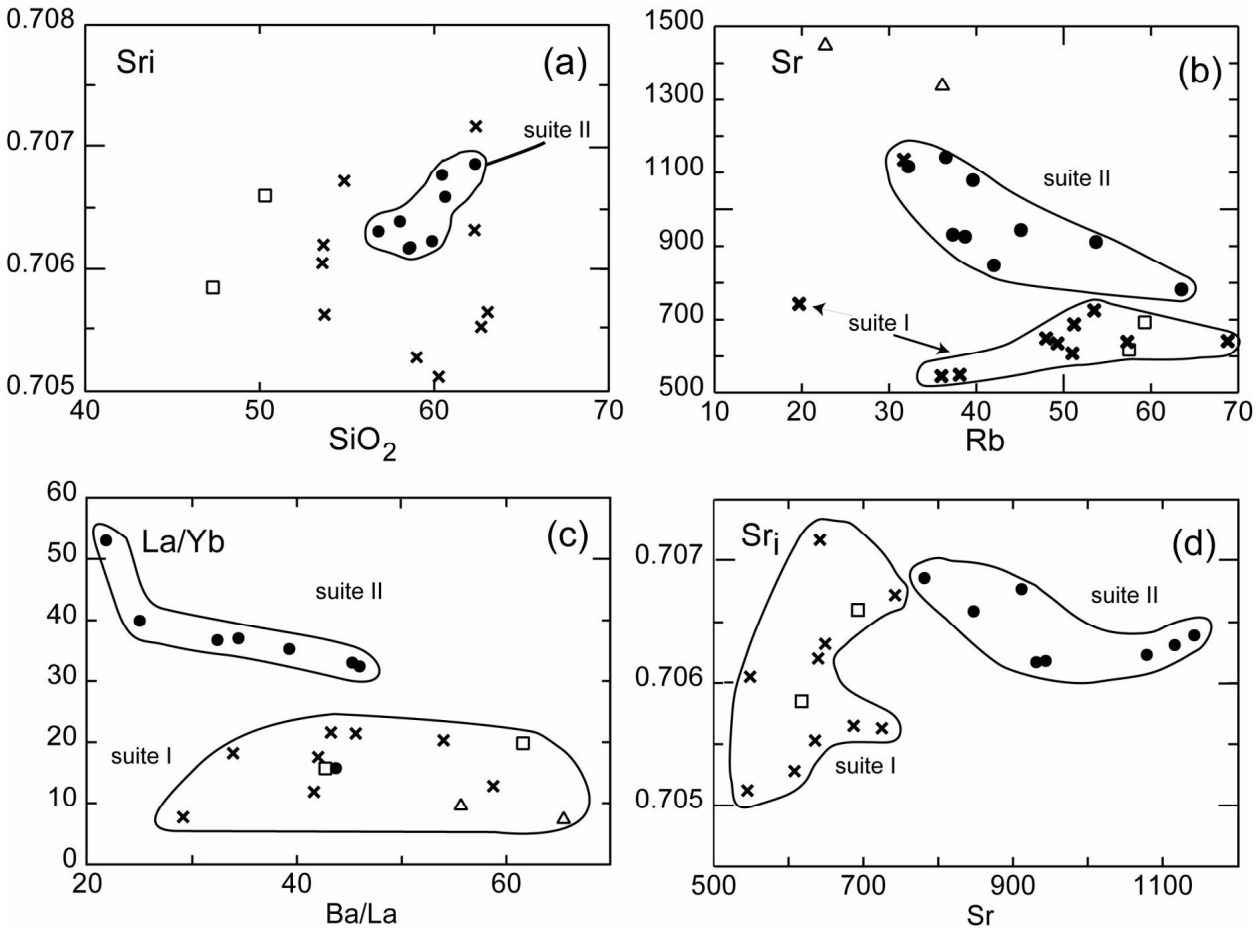

Figure 6. Trace element and Sr_i ratio discrimination diagrams that show significant differences between suite I, suite II, and the mafic enclaves and dikes. Major elements are in weight % and trace elements are in ppm. Symbols are the same as in figure 3.

Suite II

Suite II rocks have silica concentrations ranging from 58.6 to 62.3 wt. % SiO_2 (fig. 3). Silica does not correlate with geographic position. TiO_2, FeO_t, MgO, and CaO display negative and coherent linear trends with increasing silica. In contrast to other major elements, K_2O displays a strong positive and coherent linear correlation with increasing SiO_2 (fig. 3). Unlike the suite I rocks, the suite II rocks do not exhibit large variations amongst most major elements at constant silica concentrations.

Important variations in LILE are shown in figure 3. Rb concentrations display a strong positive trend ranging from 32.2 to 63.5 over the entire SiO_2 interval. Sr contents range from 1116 to 781 and display a coherent and negative linear trend throughout the silica interval. Ba has a flat trend and constant concentration (relative to suite I) ranging from 1101 to 1197 at 59 wt. % silica.

Most HFSE do not correlate well with SiO_2, but show a much narrower range in abundance at a given silica concentration than in rocks of suite I. On MORB normalized plots (fig. 4), the suite II rocks display a similar pattern as the suite I rocks but are lower in HFSE. Samples from suite II have high LILE:HFSE ratios (e. g. $Ba_N/Y_N \approx 45$) that are significantly higher than those of suite I.

The rocks of suite II have steep REE patterns with an average La_N/Yb_N of 23.1 (fig. 5, and table 3). Most patterns decrease smoothly and lack marked anomalies. No significant Eu anomalies are developed in suite II samples (see Eu/Eu*, table 3). The REE patterns for suite II are twice as steep and less variable than those of suite I. In comparison to suite I, the average REE patterns are twice as steep in suite II but have similar topologies and Eu anomalies.

The Sr_i for samples from suite II (0.70617 to 0.70686) show a weak positive correlation with increasing silica. The higher isotopic values are from the most silica-rich rocks (e. g. 22). The Sr_i for the suite II samples are less variable than the Sr_i of the suite I rocks.

Mafic Enclaves and Dikes

The mafic enclaves and the dikes are lower in silica but are similar to suite I in TiO_2, FeO_t, MgO, and K_2O (figs. 2). The enclaves and dikes plot as island arc or continental basalts on most basalt discrimination diagrams (e. g. MgO v. FeO_t v. Al_2O_3 and La/Yb versus Sc/Ni (Pearce et al. 1977)). The mafic enclaves and dikes plot over similar regions as the silica-poor rocks of suite I but are distinctly more aluminous and slightly more calcic than the host quartz diorites. Relative to the adjacent host quartz diorite, the enclave from the enclave/host pair is enriched in TiO, FeO_t, MgO, K_2O, Ba and Rb by factors of 1.5, 1.2, 1.3, 1.8, 2.4 and 3 respectively (fig. 3). However, the enclave and the host have similar concentrations of CaO, Al_2O_3, Sr, Y, and Nb. Also, the two enclaves analyzed for Sr isotopes have similar range in Sr_i as the suite I rocks (fig. 6). The Sr_i for the enclave/host pair are nearly identical suggesting isotopic equilibration between the enclave magma and the host quartz diorite.

The dikes show distinct variations from the enclaves in Al_2O_3, MgO, and K_2O at similar SiO_2 concentration. When plotted on MORB normalized diagrams, the dikes are distinguished from the enclaves by having higher Rb, Sr, Y, and Yb (fig. 4). The dikes also have different REE patterns than the enclaves where the dikes have a steeper slope (avg. $La_N/Yb_N = 11.9$) in comparison with the enclaves (avg. $La_N/Yb_N = 5.68$) (fig. 5). The enclaves and dikes have REE patterns and slopes that are similar to the suite I samples but not to those of suite II.

Summary of Geochemical and Sr Isotopic Data from Suites I and II

A Rb versus Sr diagram clearly discriminates between suites I and II (fig. 6b). The suite I rocks have Sr concentrations < 750 ppm while the suite II rocks have Sr concentrations > 750 ppm. The suite II rocks plot along a trend of increasing Rb with decreasing Sr. The enclaves are similar to the suite I rocks whereas the mafic dikes plot at even higher Sr concentrations (> 1300 ppm) than the rocks of suite II.

Suite I samples plot at lower La/Yb (~10-20) values with correspondingly higher Ba/La values (~30-70) than the samples from suite II (fig. 6c). The rocks of suite I do not define a tight trend, but occur as a coherent data cluster. In contrast, suite II defines a linear trend of decreasing La/Yb with increasing values of Ba/La. Such differences may be attributed to

interaction of the suite I magmas with mafic magmas that are low in La and high in Yb thereby shifting the suite I compositions to lower La/Yb values and higher Ba/La values. The suite II compositions are less modified by such interactions and therefore, plot at higher La/Yb values.

Rocks from suite I with the lowest Sr content also have the lowest Sr_i and define a positive trend of increasing Sr_i from 0.70512 to 0.70672 with increasing Sr over an interval of ~200 ppm Sr. In contrast, suite II rocks plot at higher Sr_i values and Sr concentrations than the rocks of suite I. Suite II samples show a weak negative trend of decreasing Sr_i with increasing Sr concentration.

As a group, rocks of the QIC broadly define a linear trend of Sr_i with a negative correlation when plotted against 1/Sr (fig. 7). The array decreases from a Sr_i of 0.70672 to 0.70512 over a wide range of 1/Sr. Suites I and II plot within separate regions of the data array. Three linear trends within suite I and II are clearly evident. Two of these trends are developed in the suite I rocks (trends A and B), and one dominant trend occurs in the suite II rocks (fig. 7).

It is clear that the two suites of the QIC are geographically, physically, geochemically , and isotopically distinct bodies. Such differences strongly suggest that rocks of suite I and II underwent different petrologic processes. The ensuing discussion uses geochemical and Sr isotopic data to assess the possible petrologic processes that resulted in the physically different suites of the QIC.

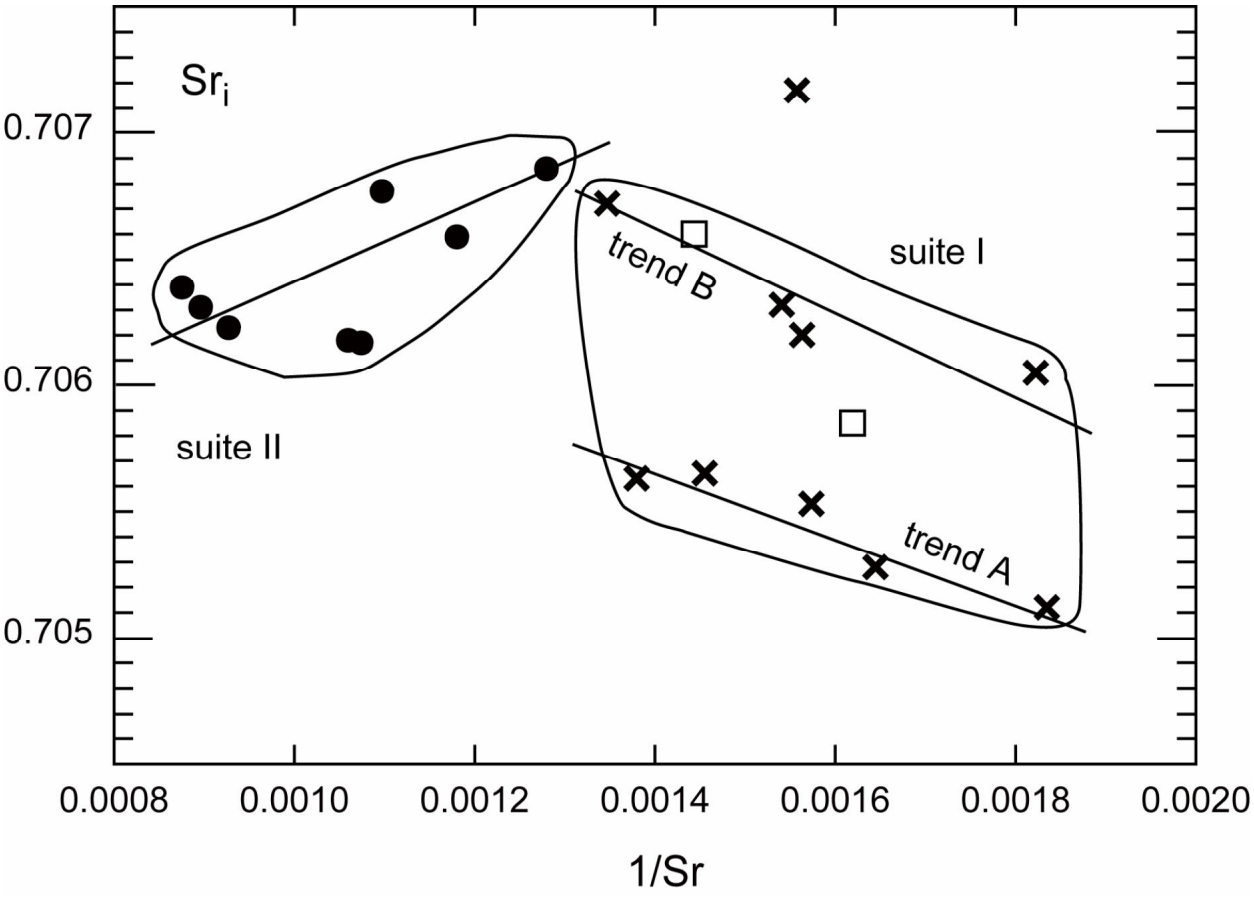

Figure 7. Plot of S_i versus 1/Sr showing two negative trends developed in suite I and a single positive linear trend in suite II. Symbols are the same as in figure 3.

Petrogenesis:

Source Region Constraints

Earlier studies by Kenah (1979) on the mechanism and physical conditions of emplacement of the QIC along the Skeena River led to a model of dehydration melting of biotite in the Central Gneiss Complex (CGC) to produce melts that formed the QIC. The melts were envisioned to have effectively mobilized the refractory source and entrained residual material (restite) during emplacement. However, neither the quartz diorites of suite I or suite II, nor the mafic enclaves/dikes preserve any physical evidence of a restite assemblage (e.g. garnet and pyroxene rimmed by plagioclase). Additionally, geochemical and Sr_i evidence indicate that the CGC is an unlikely source for the generation of the QIC. Available data (Hutchison, 1982) combined with our new data for the CGC shows that the CGC (where sampled) is more silica-rich than the QIC (fig. 8a). The melts generated from such bulk compositions would be more silicic than the QIC magmas. Furthermore, samples from the CGC analyzed for Sr isotopes yield significantly lower Sr_i (0.70459-0.70530) suggesting that the CGC is not likely to be genetically related to the QIC (fig. 8b). Since the immediately adjacent CGC is an unlikely protolith for melt derivation, other magma sources must be considered.

Detailed studies from Adak Island of the Aleutian Islands and Panamanian volcanic rocks indicate that some intermediate composition rocks, referred to as adakites, originated as melts derived from young and hot subducted slab (Kay, 1978; Defant et al., 1991; Drummond and Defant, 1991; Myers and Frost, 1994). It has been suggested that the adakitic magmas of Panama resulted from dehydration melting of amphibolitized subducted slab at 23-26 kb and 700-775°C (Drummond and Defant, 1991). The QIC and adakites have very similar major and trace element compositions (e. g. SiO_2 = 54-65 wt %, Al_2O_3 =15-19 wt % and Sr > 600 ppm). Also, the QIC plots at least partially within the adakite field on discrimination diagrams (e. g. La_N/Yb_N v. Yb_N and Sr/Y v. Y; Drummond and Defant, 1991).

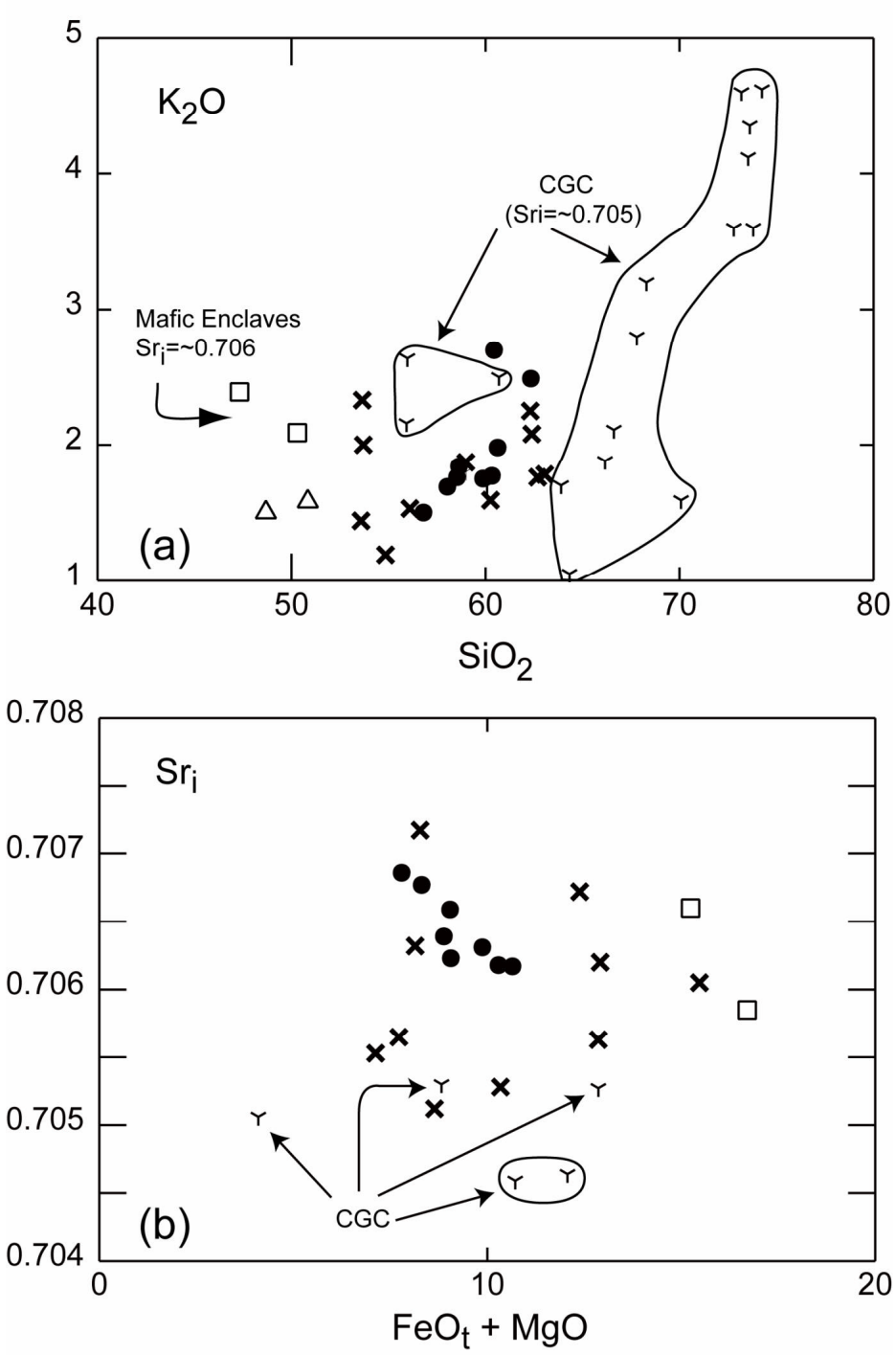

Figure 8. Discrimination diagrams showing (a) the differences in K_2O and SiO_2 between the QIC and the rocks of the Central Gneiss Complex, and (b) plot of Sr_i versus FeO_{total}+MgO for rocks of the Quottoon Igneous Complex and the Central Gneiss Complex. Central Gneiss Complex data is from this study and Hutchison (1982). Symbols for the Quottoon Igneous Complex are the same as in figure 3 and the Central Gneiss Complex is denoted by Y's.

Table 5. Trace element and REE abundances (in ppm) and Sr_i of the amphibolite used for partial melting, the assimilant concentrations used in the AFC modeling, and the basalt used in magma mixing calculations.

	Rb	*Sr*	*La*	*Ce*	*Nd*	*Sm*	*Eu*	*Gd*	*Tb*	*Dy*	*Ho*	*Er*	*Tm*	*Yb*	*Lu*	$^{87}Sr/^{86}Sr_{ic}$
amphibolite	32.1	376	16.1	36.3	22.3	6.5	2.4	7.2	1.3	7.7	1.6	4.7	0.6	4.2	0.7	0.70600
E/511	4.6	297	1.37	3.7	3.1	1.1	1.1	1.5	0.3	1.8	0.4	1.3	0.2	1.2	0.2	0.70350
assimilant	110	650	30	64	26	4.5	0.9	3.8	2.2	3.5	0.8	2.3	0.3	2.2	0.3	0.70900

Notes: The amphibolite is from the Gravina belt of S. E. Alaska; E5/11 is an island arc basalt from New Britain (Johnson and Chappell, 1979). The assimilant is a crustal composite (Taylor and McLennan, 1981). Sr_i for the assimilant and the amphibolite are model values.

However, the stability of garnet in the restite (fig. 9) at the P-T conditions of adakite formation would result in strongly depleted heavy REE abundances due to heavy REE partitioning into garnet (e.g. Kd for Lu = 41 for garnet; Irving and Frey, 1978). A discrimination diagram that uses elements strongly partitioned into garnet (Lu, Yb, Y) clearly separates adakitic magmas from those of the QIC emphasizing the extreme HREE depleted signature of adakitic magmas (fig. 10). Also, it is unlikely that the isotopically evolved compositions of the QIC magmas were derived directly from an isotopically primitive mantle source (e. g. Sr_i <0.7045). Therefore, we suggest that the QIC magmas were probably not derived from partial melting of a subducted slab.

Experimental evidence suggests that the major element abundances similar to those of the QIC (fig. 11) can be generated by partial melting of amphibolite compositions (Beard and Lofgren, 1991; Rushmer, 1991; Wolf and Wyllie, 1994; Patiño Douce and Beard, 1995). Metamorphosed mafic lithologies (amphibolites) have a range of Sr_i that are commonly similar to those of the parental magma for the QIC (i.e. ~0.706) (Sinha and Davis, 1971; Samson, 1990;Wendlandt, et al., 1993; Borsi et al, 1995). Experimental partial melting of amphibolites demonstrates that large volumes of melt (20 to 50 %) may form in a variety of tectonic environments over a range of crustal P-T conditions (3 to 15 kb and 850-1000°C) resulting in low potassium melts with intermediate compositions. The restite assemblages from these experiments (and their phase equilibria) provide constraints on the trace and REE composition of intermediate magmas. As demonstrated experimentally, different restite assemblages form at different pressure and temperature conditions and garnet increases in importance as a residual phase at pressures above ~10 kb (fig. 9) (Beard and Lofgren, 1991; Rushmer, 1991; Wolf and Wyllie, 1994; Patiño Douce and Beard, 1995; Winther, 1996). Also, dehydration melting experiments show that plagioclase decomposes at pressures ~14 kb (the plagioclase out boundary). Therefore, partial melting of an amphibolitic source reservoir at pressures >10 kb at or near the plagioclase out boundary (~14 kb) could result in the elevated Sr and the HREE depleted nature of the QIC magma.

Modeling of batch partial melting (Shaw, 1970) of an amphibolite (table 5) is used to assess the changes in REE abundances produced by partial melting of mafic protoliths. The model uses published partition coefficients (Philpotts and Schetzler, 1970; Schnetzler and Philpotts, 1970; Gill, 1981). The model melts have a restite assemblage containing pyroxene,

garnet, apatite, sphene , and zircon (see fig. 12 for percentages) which are similar to those produced during experimental partial melting of amphibolites at P≥10 kb (Wolf and Wyllie, 1994; Patiño Douce and Beard, 1995). Forty percent melting (fig. 12) produces melts that have similar La_N/Yb_N slopes (20.9) and Eu/Eu* (1.19) to those found within suite II (e. g. avg. La_N/Yb_N=23 in suite II; see table 3). Because crystal fractionation of major silicate phases and/or accessory phases only has minor influences on La_N/Yb_N, this ratio is a direct function of garnet in the restite assemblage (see below). The QIC has slightly lower middle REE abundances than those predicted by the partial melting model. This study suggests that crystallization and settling of the accessory minerals apatite and sphene from the magma after removal from the source region strongly affected the middle REE abundances.

Thus the geochemical data and the model suggest that the parental magma composition for the QIC was generated by dehydration melting of amphibolitic compositions at pressure and temperature conditions of >10 kb and ~1000°C. At these conditions garnet and pyroxene were stable and amphibole and plagioclase were not stable in the restite assemblage. The major element chemistry from experimental partial melting of amphibolite agrees well with the parental composition of the QIC; steep REE patterns suggest a high pressure source (> 10 kb) where garnet was a stable residual phase; the REE patterns are not as steep as those of adakites (adakites have La_N/Yb_N >30); and high Sr contents (suite II avg. = 981 ppm, and up to 1135 ppm) imply that the source was near the plagioclase out boundary at ~14 kb. The Sr_i of the parental material is measurably higher than mantle values and further supports a crustal source as a protolith.

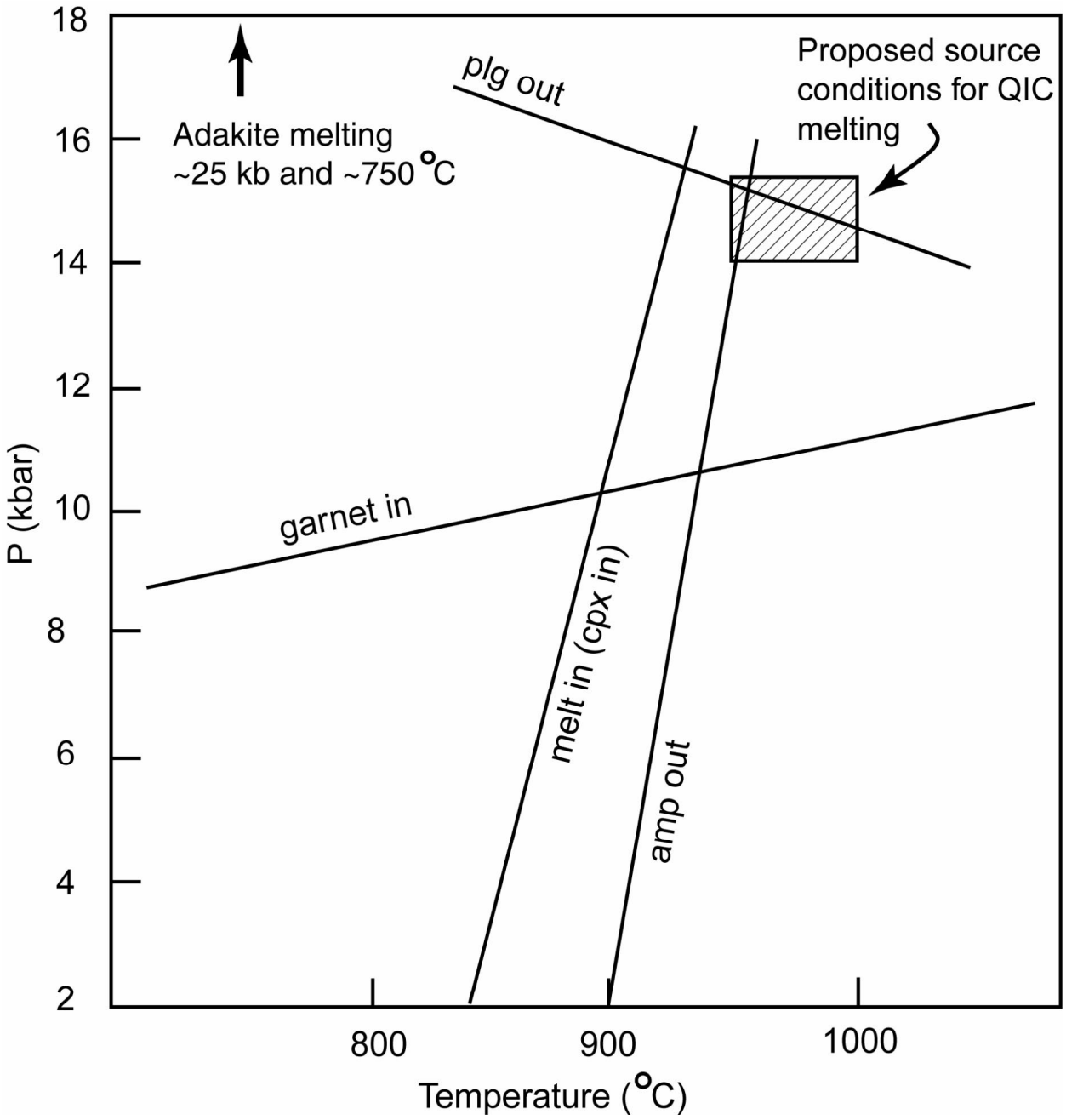

Figure 9. Experimental phase relations for dehydration melting of amphibolitic protoliths (experimental data from Beard and Lofgren, 1991; Rushmer, 1991; Wolf and Wyllie, 1994; Patiño Douce and Beard, 1995; Winther, 1996). Location of the proposed P-T conditions for the formation of the parental QIC liquid prior to magma mixing and AFC processes is outlined in the box. gt=garnet, plg=plagioclase, opx=orthopyroxene, cpx=clinopyroxene; line labeled melt is the solidus.

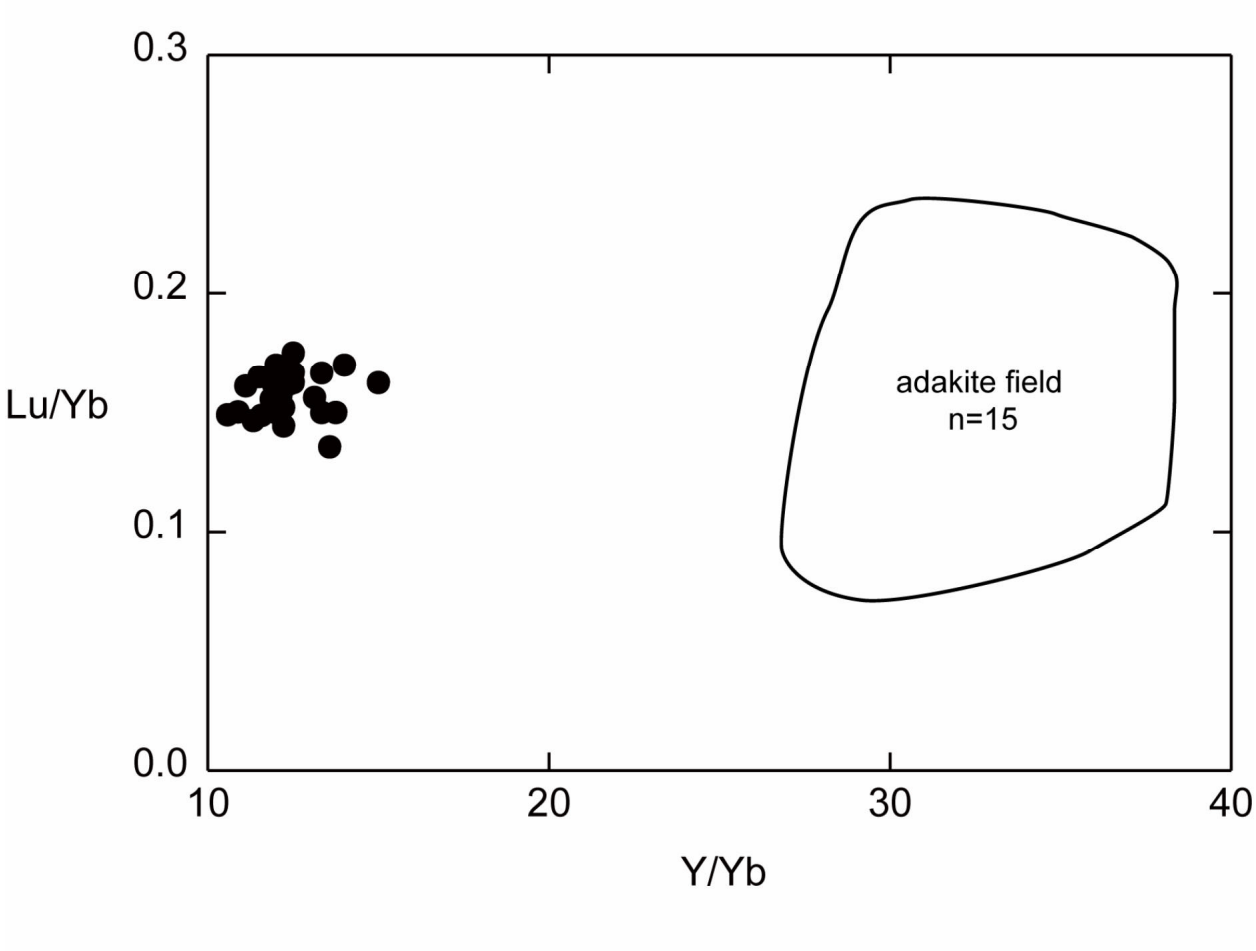

Figure 10. Discrimination diagram that shows the heavy rare earth element depleted nature of adakitic magmas derived through melting of a young subducted oceanic plate. The heavy rare earth element depleted nature of the magmas is due to increased garnet stability at higher pressures. The Quottoon Igneous Complex data (solid circles) have a much lower Y/Yb ratio suggesting significantly less garnet in the restite during partial melting. Adakite data (n=15 analyses) is from Drummond and Defant, 1991; Defant and Drummond; Barker, 1979; Myers and Frost, 1994.

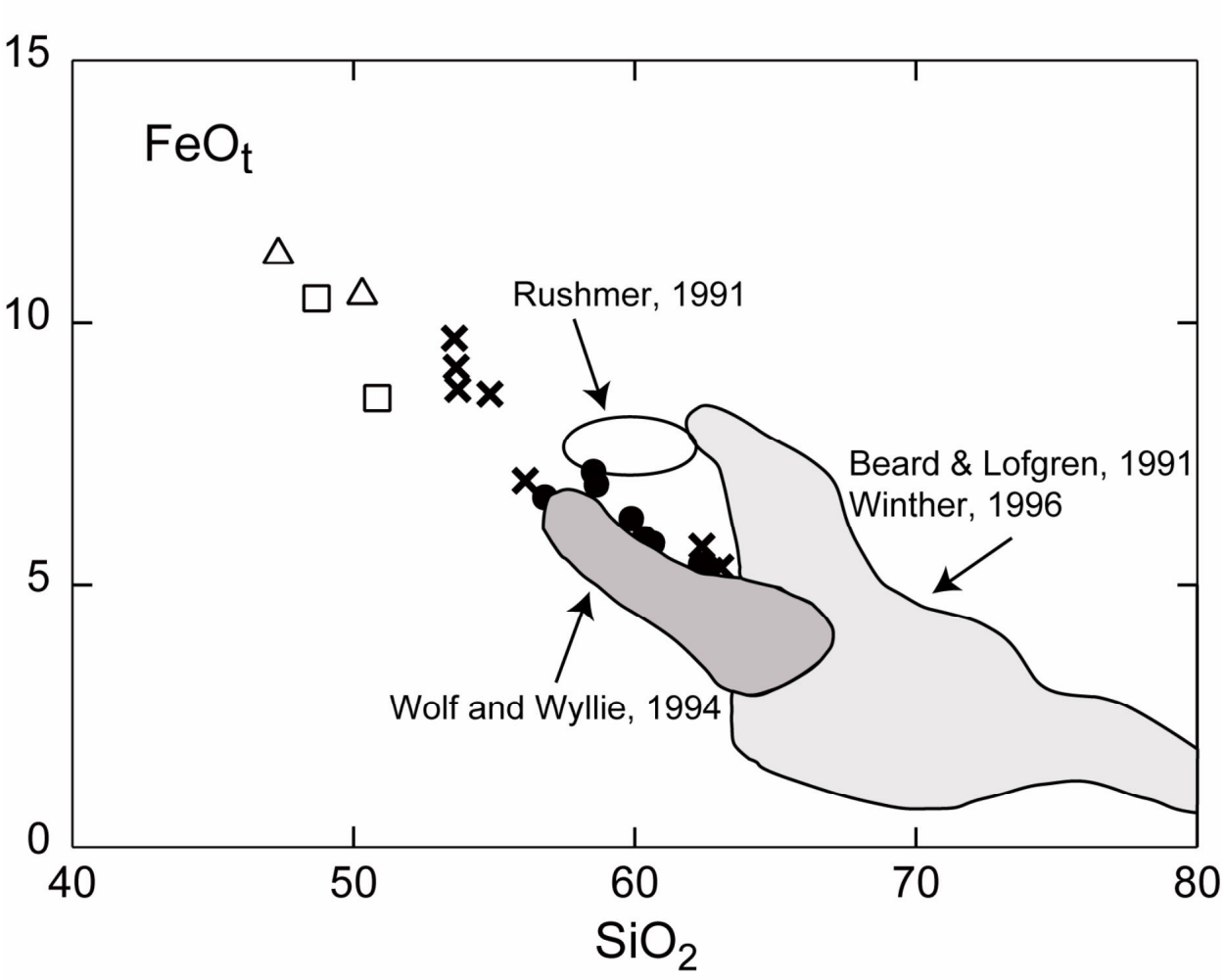

Figure 11. Major element abundances (normalized to 100 wt. % anhydrous) for 20 to 50 % partial melting of amphibolitic compositions that yield melts similar to those of the Quottoon Igneous Complex. Symbols are the same as in figure 3 and experimental data are from references listed in the diagram.

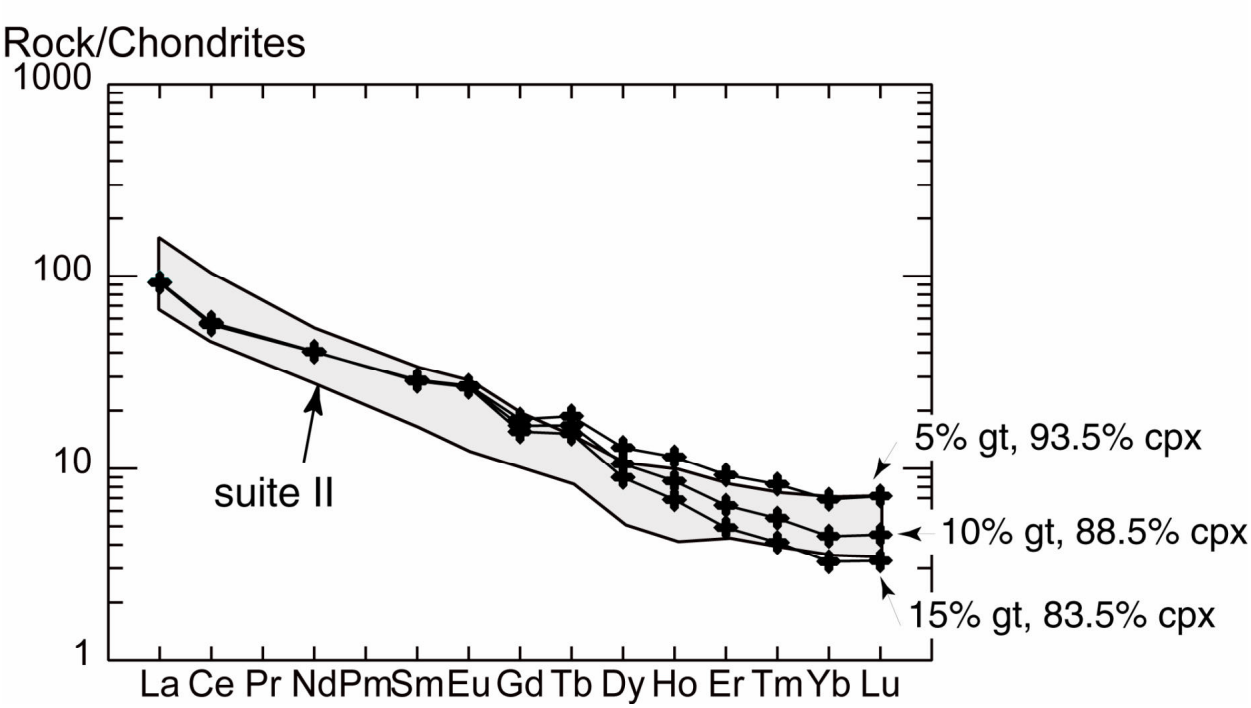

Figure 12. REE modeling of partial melting of an amphibolite (table 5) with a variable restite assemblage containing variable amounts of garnet, clinopyroxene, and apatite (percentages listed in the figure). Although similar La_N/Yb_N are generated from model melts, the middle REE do not correlate well with the QIC. The shaded field is the range of REE abundances from suite II. The crosses are the model compositions.

QIC Evolution after Parental Magma Generation

The range of compositions observed for the suite II rocks is best modeled by processes involving fractional crystallization. Least squares calculations using mineral data from Kenah (1979) were performed to reconcile the major element abundances. Sample 55 is used as a parental composition because: 1. it is similar in composition to experimental amphibolite melts (Beard and Lofgren, 1991; Rushmer, 1991; Wolf and Wyllie, 1994; Patiño Douce and Beard, 1995; Winther, 1996) and 2. it has a low silica concentration that may be parental to more felsic compositions. Although the low R^2 values from the calculations (0.03) (see Defant and Nielsen 1990 for assessment of R^2 values) suggest that fractional crystallization is a likely process that could produce the range of compositions of suite II, the range in Sr_i precludes this process. In an attempt to reconcile the Sr_i and geochemical data, suite II rocks were modeled utilizing assimilation and fractional crystallization processes (AFC) (DePaolo, 1981) using the same parental composition as above (sample #55). The assimilant has a fixed composition that is similar to average continental crust (table 5) (Taylor and McLennan, 1981). Results of the calculations obtained through removal of an assemblage containing 65 % plagioclase, 34 % hornblende, 0.3 % sphene, 0.5 % apatite, and 0.2 % zircon are shown in figures 13 and 14 using published partition coefficients (Philpotts and Schnetzler, 1970, Schnetzler and Philpotts, 1970; Drake and Weill, 1975; Green and Pearson, 1985a; Fujimaki, 1986). Forty percent fractionation of the above assemblage with concurrent assimilation (r=0.3) provide a reasonable explanation for the correlations developed in suite II between SiO_2, Rb, Sr, Nb, the REE and Sr_i (fig. 5a-c). The Rb-Sr-Sr_i relationships are well constrained by AFC processes (fig. 13a and b) and support the fractionation of the above assemblage. Model melt composition produced from amphibolite partial melting (in above section) have higher chondrite normalized values for the middle REE than those measured for the suite II rocks (fig. 12). AFC processes that remove apatite, sphene, and zircon from the liquid would result in REE patterns and abundances similar to those of the suite II rocks (fig. 14). The samples that do not fit well to the AFC trend may be explained through: (i) a changing bulk distribution coefficient during crystallization (Ragland, 1989), (ii) two separate parental magmas within suite II, or (iii) differing rates of assimilation(r=1 to r=4) during crystallization.

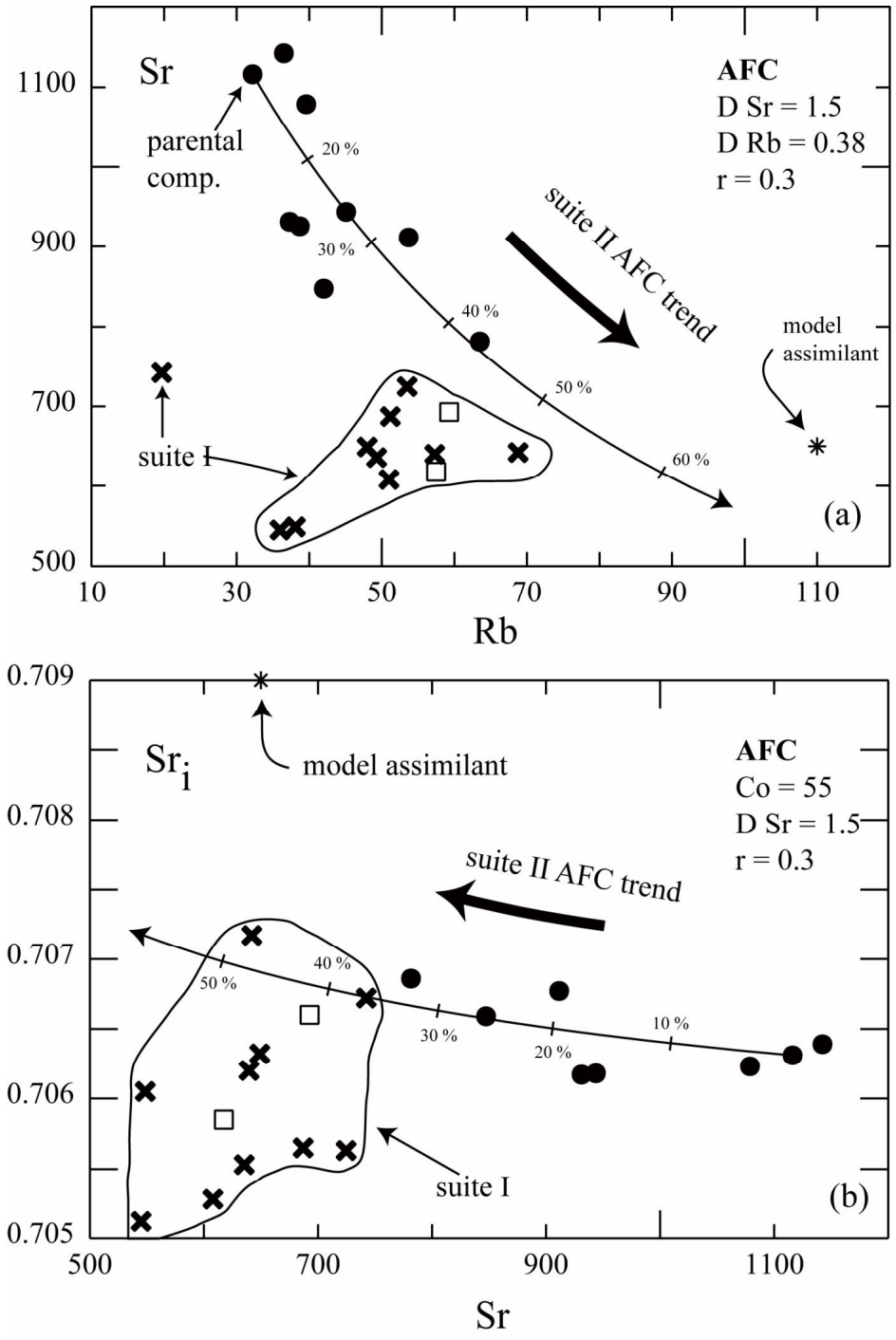

Figure 13. (a) a plot of Rb versus Sr and (b) Sr_i versus Sr. Both diagrams show the compositional trends generated by assimilation and fractional crystallization processes. The model assimilant (shown as an asterisk) is a crustal composite from Taylor and McLennan (1981). The Sr_i for the assimilant is a model value. Symbols for the QIC are the same as in figure 3.

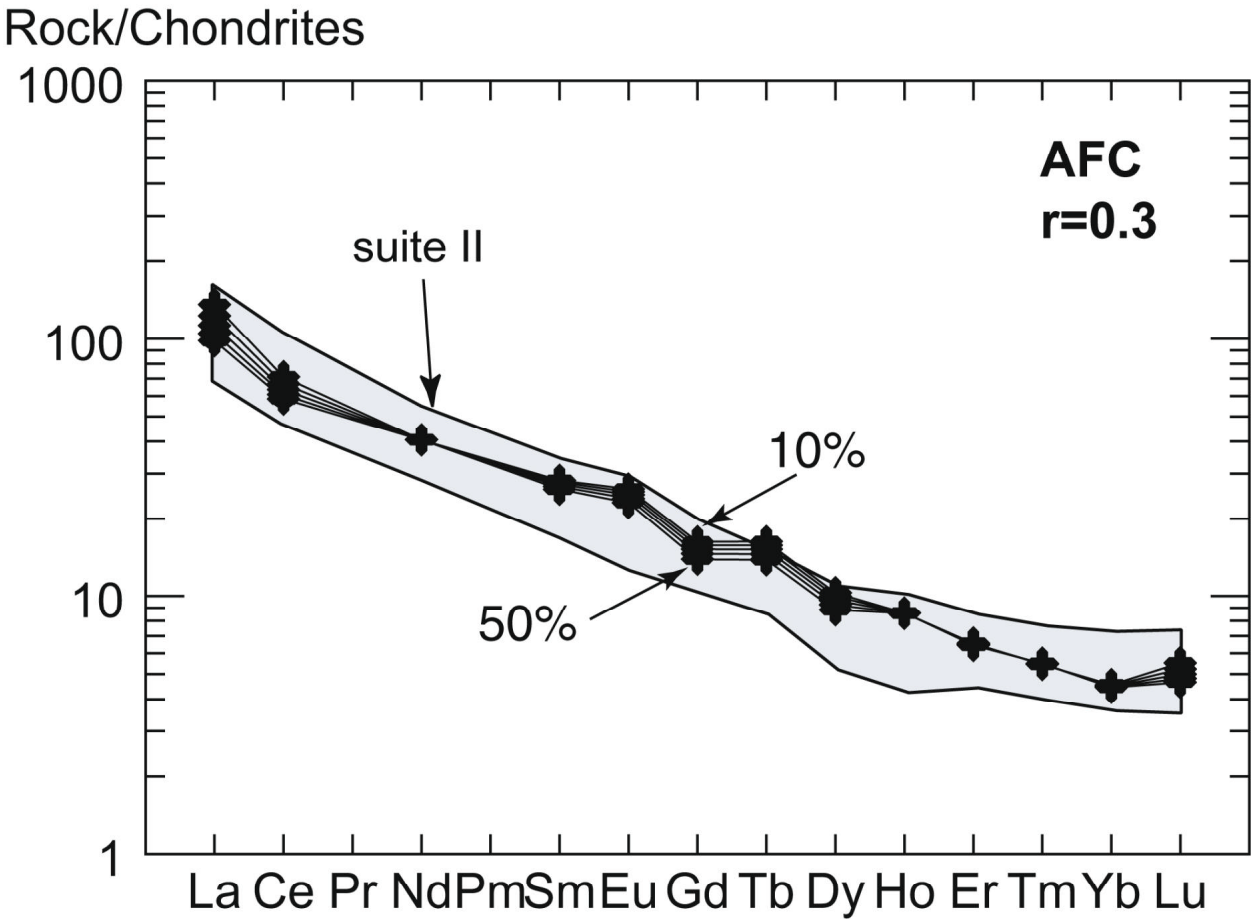

Figure 14. REE modeling of AFC processes (10-50 % fractionation) where 62 % plagioclase + 33 % hornblende 1% sphene + 3 % apatite + 1 % zircon are removed from the model melt composition produced from the partial melting model shown in figure 12 (10 % garnet restite). The shaded field is the range of REE abundances from suite II and the crosses are the calculated model compositions.

Fractional crystallization involving plagioclase did not cause significant Eu anomalies possibly due to: 1. small bulk distribution coefficient for Eu (1.02) due to the opposing effects of partitioning into hornblende and plagioclase, 2. plagioclase accumulation, 3. the oxidation state of Eu (2+ or 3+). The assemblage sphene + magnetite + ilmenite records the oxidizing conditions of the magma. At high oxygen activities it is likely that Eu may have behaved incompatibly as Eu^{3+} (Drake and Weill, 1975; Wones, 1981, 1989; Rollinson, 1994).

At the level of emplacement, there is no field evidence for extensive assimilation in the form of abundant and reacted xenolithic material in the QIC. Furthermore, the wall rocks of the QIC (CGC, samples 893,1593, 1293, 38GMO) consistently yield relatively low values of Sr_i (0.70434-0.7053; see table 4) and therefore did not contribute to the isotopically evolved nature of the QIC as a radiogenic assimilant (fig. 6). Therefore, it is likely that assimilation of radiogenic lithologies that affected suite II must have occurred below the level of emplacement.

The more heterogeneous rocks of suite I can not be modeled through fractional crystallization or AFC processes. In addition to high R^2 values (>0.1) for least squares calculations and the Rb-Sr relations, a large range in Sr_i suggests that fractional crystallization is not the dominant igneous process that affected suite I. The suite I rocks do not lie along any fractional crystallization or assimilation and fractional crystallization (AFC) trends, but instead they occur as clusters of data that have a trend opposite to that expected from fractional crystallization (fig. 13 a and b) (i. e. decreasing Sr with increasing Rb and Sr_i for AFC processes).

The abundance of mafic enclaves and dikes in various stages of disaggregation and reaction in suite I suggest that the magma chemistry may have been affected by magma mixing processes (Vernon, 1983; Allen, 1991, Blundy and Sparks, 1992; Holden et al., 1991). Many enclaves appear to have reacted with the host magma and occur only as 'ghosts' with diffuse margins. The heterogeneous textures (fine-grained material mixed with coarser-grained material) and strongly reacted hornblende (sieve textures) of quartz diorites proximal to enclaves and dikes suggests enclave/host interaction (Vernon, 1983). In addition, highly variable geochemical and Sr isotopic compositions, and the equilibrated Sr_i between the enclave and its host (from the enclave/host pair, see table 4), suggests the likelihood that magma mixing was an important process in the petrogenesis of suite I.

Calculations using the equations of Langmuir et al. (1978) were used to assess magma mixing as well as the proportions of quartz diorite and the mafic endmember components involved in the mixing process. We assume that the mafic mama involved in mixing is basaltic in composition due to the general trend of the Sr_i towards mantle isotopic compositions. The mafic endmember composition used in the model (table 5) is an island arc basalt from the New Britain arc (Johnson and Chappell, 1979). The mafic enclaves and dikes were not chosen as the mafic endmembers because they have interacted and equilibrated to varying degrees with the host quartz diorites; therefore, they have inherited physical, geochemical, and isotopic characteristics from the host.

A plot of Rb/Ca versus K/Sr (incompatible element/compatible element) displays a parabolic mixing curve (fig. 15a) between the highest silica sample (#72) from suite I and the hypothetical mantle derived endmember. The majority of the samples can be explained through a mixture containing <45 % IAB magma emplaced into a quartz dioritic liquid. However, no simple mixing line exists that includes all of the data. Also, suite I rocks do not define a single mixing line when Sr_i is plotted against 1/Sr, but rather the data define two trends (trends A and B) (fig. 15b). Compositions along trend A can be produced through a mixture containing <65 % mantle-related magma mixed into the QIC parental composition (sample #55, of suite II). A mixture containing <45% mantle endmember mixed with the most evolved sample from suite I (#72) can produce the compositions along trend B. The absence of a single mixing line could have been produced through accumulation, fractional crystallization, or AFC processes where the hybrid magmas continued evolution after mixing. In this case the original magmas comprised a single mixing line which underwent subsequent modification due to continued magmatic evolution through AFC processes (see Myers and Sinha, 1983; Myers and Frost, 1994). AFC processes would generate a trend of increasing Sr_i with increasing 1/Sr (fig. 16). Just as likely, the felsic endmember may have changed composition due to fractionation processes prior to magma mixing so that the felsic endmember continually fractionated throughout the mixing interval. It is not possible to discriminate between these environments. Regardless of the sequence of mixing events that affected suite I, it is clear that the data define an envelope of combined processes dominated by magma mixing with minor fractionation processes.

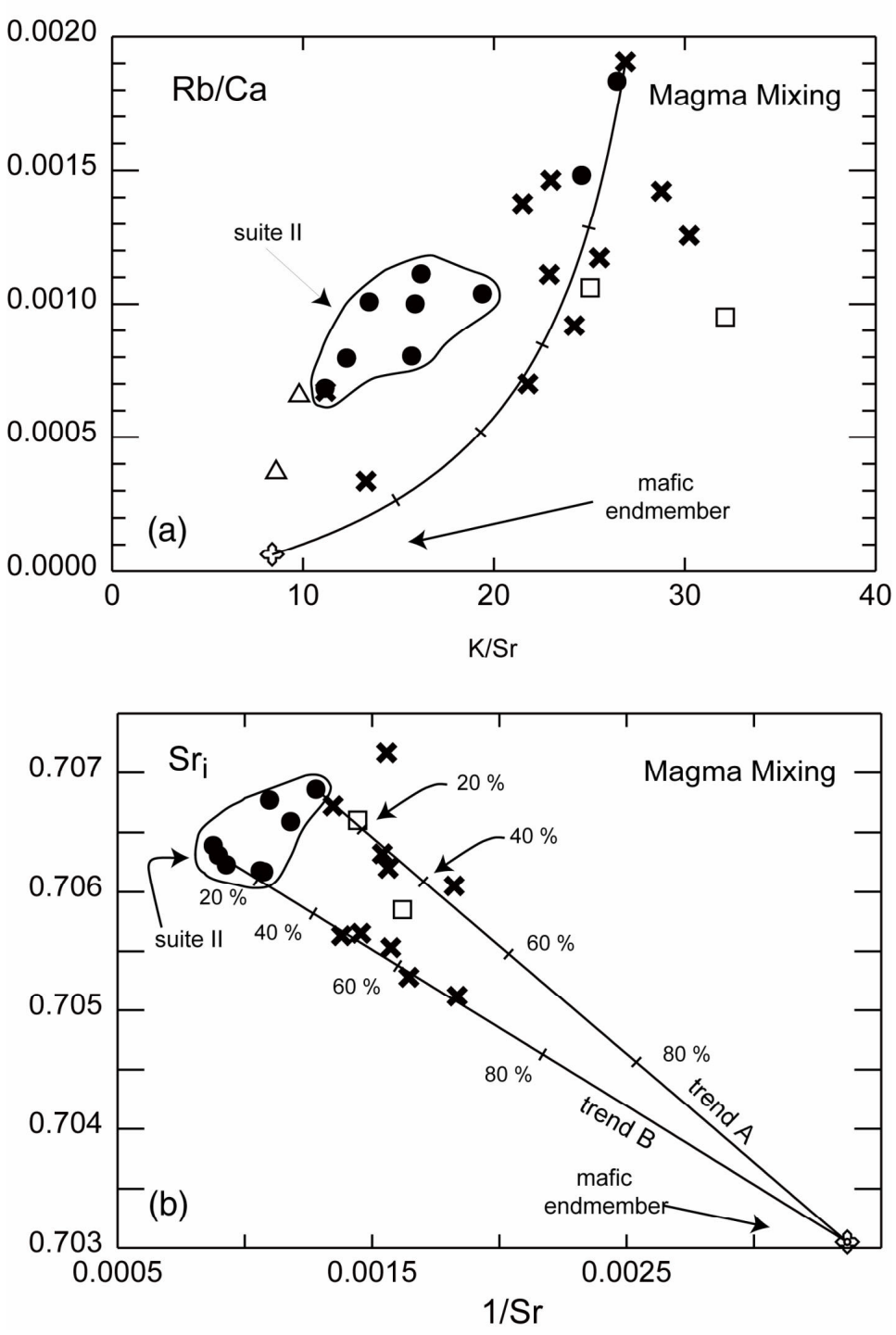

Figure 15. Diagrams illustrating the effects of magma mixing using (a) the most felsic composition from suite I and an island arc basalt from New Britain (the cross is sample E5/11 from Johnson and Chappell, 1979; table 5) as the mafic endmember, and (b) the isotopically most evolved sample from suite II to generate trend A and the most isotopically most primitive sample from suite II to generate trend B. Symbols are the same as in figure 3.

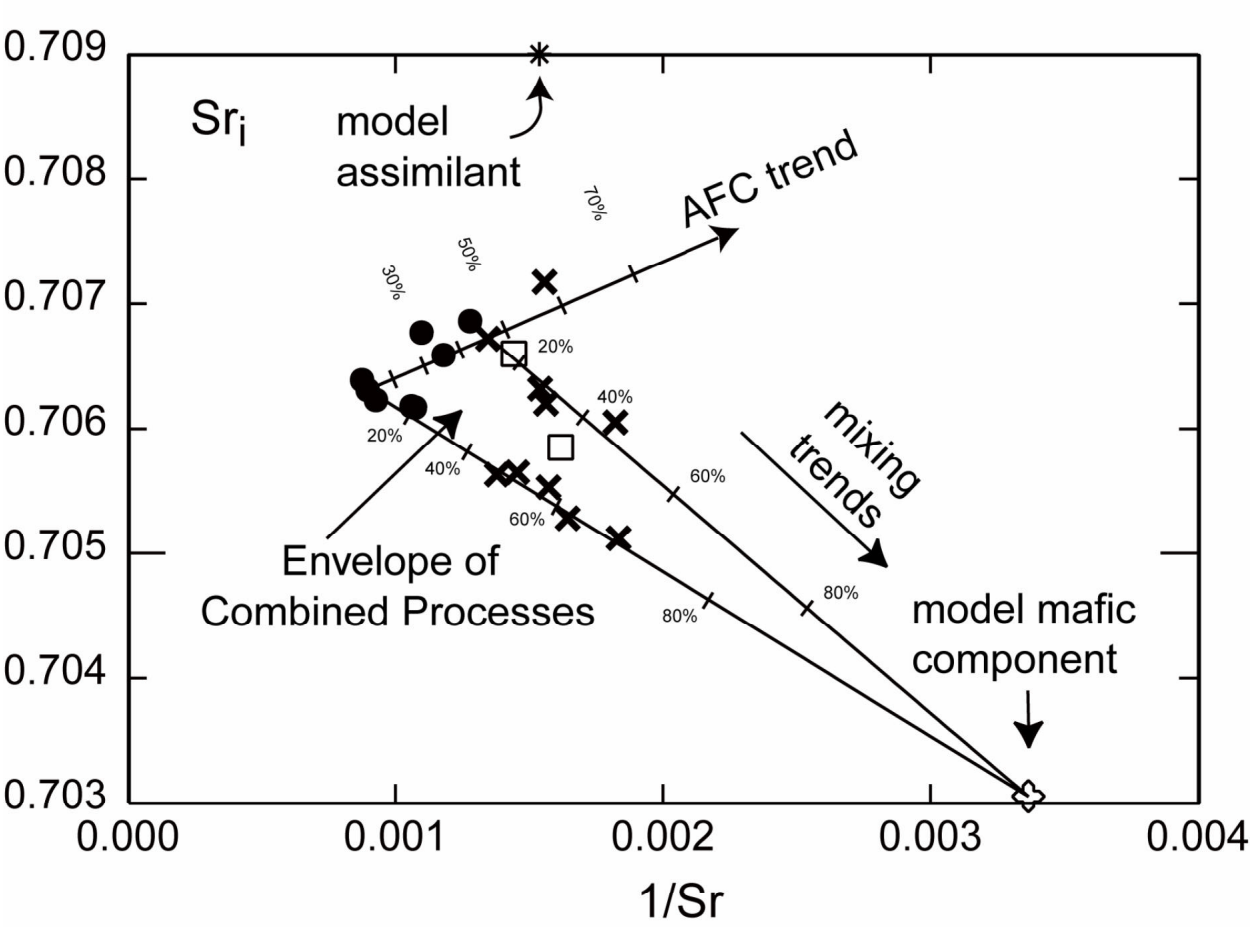

Figure 16. Diagram showing a dynamic model of magmatic evolution for the QIC. The suite I rocks may have originally comprised a single mixing line with the mafic endmember prior to subsequent evolution through fractionation processes or the mafic endmember may have mixed with a felsic endmember that was undergoing AFC processes during magma mixing. The mafic endmember is the same as in figure 13 and symbols are the same as in figure 3. See text for discussion.

Relationship to the MASH Hypothesis

The two suites of the QIC provide the opportunity to assess changes in geochemical and isotopic characteristics established in orogenic magmatic systems. The heterogeneous suite I rocks were probably produced in an environment where abundant mantle-derived magma caused lower crustal melting and the mantle-derived magma was subsequently injected into the quartz dioritic melt where it mixed incompletely prior to and during emplacement. Such processes resulted in the physical, geochemical and isotopic heterogeneity within suite I. In contrast, the suite II rocks are physically, geochemically, and isotopically more homogeneous than those of suite I. The decreased importance of magma mixing in suite II suggests that the measured compositions reflect more closely the geochemical nature of the source region.

Hildreth and Moorbath (1989) describe a mechanism for the formation of intermediate magma through processes of melting, assimilation, storage, and homogenization (MASH). A variety of methods were provided to discriminate between mantle and crustal signatures of magmas involved in the MASH process. The following features are attributed crustal processes: elevated Ba/La, high Sr_i ratios, variable Ba/Ta, low K/Rb, large shifts in Rb/Zr, low HREE and high concentrations of Hf and Ta. In contrast, they attribute low Ce, enriched HREE, high La/Ta, elevated Ba/Th, low Zr/Nb, and high Nb/U to contributions from the mantle wedge. The mid-crustal QIC provides a window that avoids the influence of upper crustal processes at structural levels closer to the MASH zone.

The MASH parameters are in good agreement with previously described geochemical data suggesting that the QIC was indeed derived from a lower crustal source. However, this study extends the MASH model to further constrain individual processes that can affect magma chemistry through time. This study suggests that at least two different igneous processes are recorded in the QIC. The mixed rocks of suite I record extensive interaction of mantle-derived magmas with lower crustal lithologies while suite II records a crustal melting process with less mantle interaction/addition.

An Evolutionary Model for the QIC

Although the suite I rocks are not useful in constraining the pressure, temperature and composition of the source region, they provide a window into lower crustal processes that may be responsible for initiation of magmatism. Abundant mafic enclaves and dikes observed in the field, and estimates using geochemical and isotopic modeling suggest that a large volume of mantle-related magma was involved in the petrogenesis of suite I (up to 65 %). In addition to the extensive chemical modification sustained in suite I rocks, it is likely that intrusion, ponding, and/or underplating of mantle-related magmas in the lower crust may have provided some of the heat necessary for magma generation in the amphibolitic reservoir. The proposed model for magma genesis and subsequent evolution of the QIC involves five stages and three geochemical/isotopic components:

1. Crustal thickening and elevation of the pressure and temperature conditions (Crawford et al., 1987).
2. Interaction of lower crustal amphibolitic lithologies (component A) with mafic mantle-related magmas (component B).
3. Dehydration partial melting of amphibolitic compositions in the lower crust to generate a parental quartz dioritic QIC magma.
4. Dynamic interaction and mixing (with minor AFC) between the mantle-related magmas and the QIC parental magma produced the extensively modified and enclave-rich suite I.
5. Suite II was produced by decreased interaction with mafic mantle-related magmas and subsequent evolution through fractional crystallization with minor assimilation (AFC) of a relatively radiogenic component (component C).

Such a model for the evolution of the QIC is in good agreement with tectonic constraints from regional metamorphic and structural investigations. Derivation of mantle related melts, high grade metamorphism, and uplift of the Coast Plutonic Complex are attributed to collision and underthrusting of the Alexander/Wrangellia terranes with the Stikine/Yukon-Tanana terranes during the mid-Cretaceous (Crawford and Hollister, 1982; Crawford et al., 1987; Rubin et al., 1990; Samson et al., 1991). It has been suggested that thrust related deformation and crustal

thickening ended at approximately 90 Ma (McClelland, 1990). The time lag between the end of crustal thickening and the initiation of Coast Plutonic Complex magmatism (from 65-50 Ma) is similar to the 40 Ma lag time predicted from thermal modeling of crustal thickening (England and Thompson, 1984; Armstrong, 1988; Zen, 1988b; Patiño Douce et al., 1990). Crustal thickening may have elevated the temperature in the lower crust so that subsequent ponding, underplating, and/or intrusion of mantle-related magmas into the lower crust could have resulted in large-scale magma generation (Huppert and Sparks, 1988). After partial melt formation from amphibolitic lithologies in the lower crust, extensive interaction between mafic mantle-related magmas and lower crustal melts resulted in the development of the mixed suite I rocks. Emplacement of this mixed magma then occurred along the CSZ during its waning stages of convergent tectonics (e. g. Klepeis and Crawford, 1996). As a result, the heterogeneous suite I rocks were deformed producing the large x:z ratios of mafic enclaves, well developed foliations, and solid-state deformation features (e .g. subgrain formation). The final stage of QIC evolution involved decreased interaction of mantle-derived magma and emplacement of suite II may have occurred along the CSZ during a non-compressional stage. Thus, the QIC provides a record of magmatic evolution that coincides with tectonic evolution along the Coast Shear Zone.

Comparisons to Plutons from the Great Tonalite Sill

Physical and geochemical investigations of other Paleogene plutons from the Great Tonalite Sill (GTS) near Juneau, AK (fig. 1) indicate that some plutons contain structurally distinct sheets of tonalite (Drinkwater et al., 1989; Drinkwater et al., 1990; Gehrels et al., 1991; Brew, 1994; Drinkwater et al., 1995; McClelland and Mattinson, in press). The Speel River, Mount Juneau, Annex Lakes, and Lemon Creek Glacier plutons contain much more potassium feldspar than the QIC. However, all plutons overlap the silica range of the QIC and the Speel River pluton even shows an apparent silica discontinuity with the most mafic rocks contained in the western portion of the pluton. Earlier studies (Gehrels et al., 1991) suggest that Ferebee, Carlson Creek, and the tonalite in Tracy Arm may be composite in nature based on geochronologic data. Furthermore, the Sr_i data from the GTS shows significant variation ranging from 0.70494 at Tracy Arm to 0.70640 at Thomas Bay (Arth et al., 1988; Samson et al., 1991). The Rb, Sr, and Sr_i data from the other plutons of the GTS (fig. 17) show similarities to suite I rocks of the QIC and suggest that they may have formed through similar mixing processes. Using the same endmembers as used in the mixing models for suite I, the compositions of the plutons from the GTS can be explained through mixtures containing up to 65 % of the mafic mantle-related component.

Nd, and Sr investigations and the identification of inherited zircon components in the northern Coast Mountains led to a petrogenetic model involving partial melting of mafic lower crustal lithologies and subsequent interaction with subduction-related mafic magmas to produce the plutons of the GTS (Arth et al., 1988; Gehrels et al., 1991; Samson et al., 1991). A range in Sr_i and initial values of εNd = -0.9 to -3 from other portions of the Great Tonalite Sill in southeastern Alaska support such a model. The Nd isotopic studies suggest that the GTS rocks contain an ancient and isotopically evolved component (25 to 50 %) attributed to the Yukon-Tanana terrane. The components as proposed by Samson et al. (1991) are similar to the crustal- and mantle-related endmembers developed in this study. It is currently unclear to which terrane the source region of the QIC belongs. However, these models corroborate physical, geochemical, and isotopic data from this study suggesting that extensive interaction occurred between a mantle-related magma and a more evolved intermediate crustal-related magma derived from partial melting of lower crustal amphibolitic lithologies. The modeled proportions

of mantle-related material involved in the petrogenesis of the QIC is similar to the proportions proposed by Samson et al. (1991). Abundant physical and geochemical information from this and other investigations show that magma mixing is a significant and regionally extensive process that operated throughout the entire GTS. Since the QIC is one of the largest plutonic bodies of the GTS and sufficient field, petrologic, and isotopic/geochronologic data exists, the processes preserved within the rocks may be regarded as a petrogenetic reference for comparing Paleogene magmatism throughout the GTS belt.

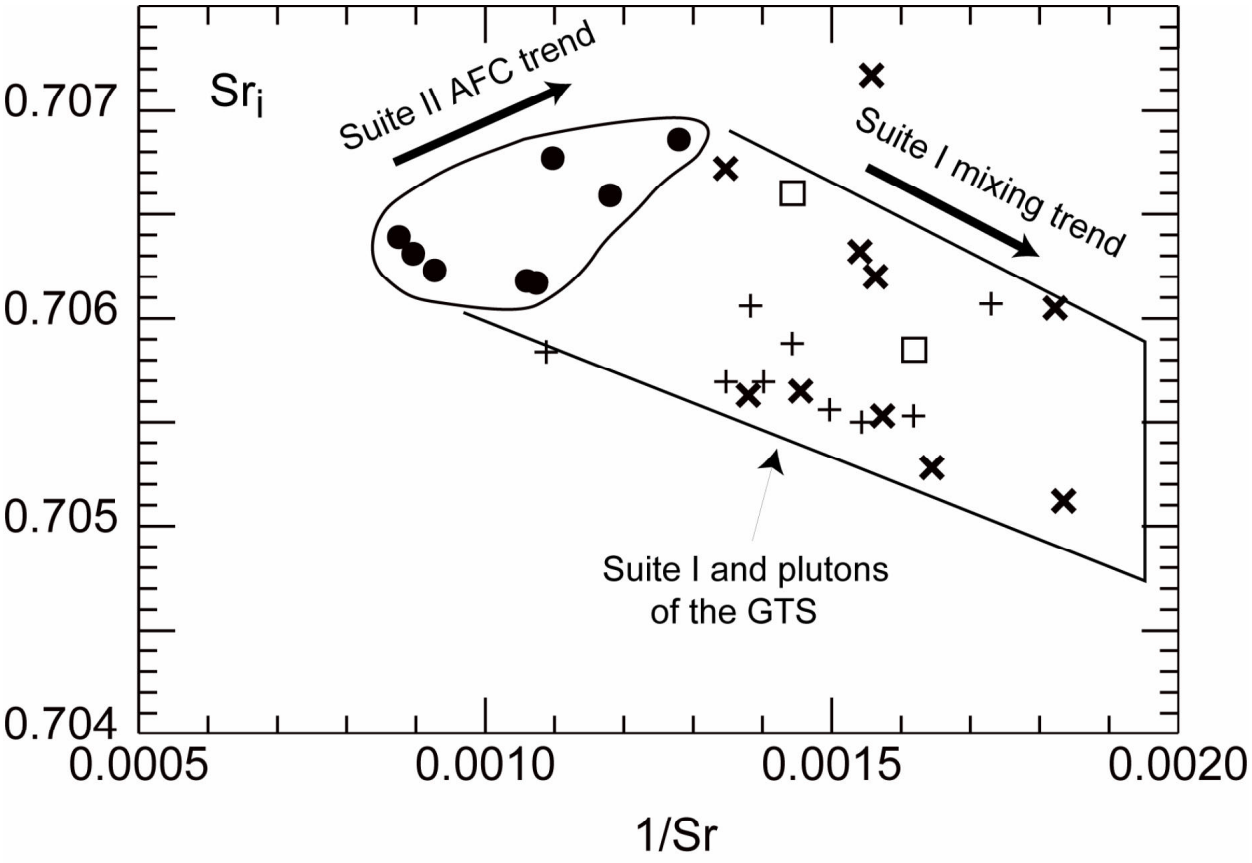

Figure 17. Diagram comparing the QIC to other plutons of the Great Tonalite Sill (GTS). Crosses denote samples from plutons of the GTS (Samson et al., 1991) and symbols for the QIC are the same as in figure 3.

Conclusions

Differences in field, petrographic, geochemical, and isotopic data from the quartz dioritic Quottoon Igneous Complex show that it consists of two distinct suites. The suites are physically distinct. Suite I is pervasively deformed and contains abundant mafic dikes and enclaves. The enclaves are elongate and parallel the well-developed foliation. Interaction with the mafic enclaves and dikes has modified the quartz dioritic magmas and resulted in the heterogeneous nature of suite I rocks. Geochemical and isotopic data indicate that the dominant petrologic process that operated in suite I was magma mixing in which a mantle derived basaltic magma extensively modified a more felsic magma derived from partial melting of amphibolitic lithologies. Such processes resulted in the physically and chemically heterogeneous rocks of suite I. The suite I rocks do not define a simple mixing line between the mafic magma and the more quartz dioritic endmember as expected for a two-component mixture. Deviations from a single mixing line are attributed to continued evolution after magma mixing through fractionation or AFC processes. Alternatively, the endmembers may have continually evolved throughout magma mixing processes. Modeling of geochemical data using magma mixing as a process suggests that the suite I rocks contain up to 65 % of a mafic magma mixed with a quartz dioritic magma. The mafic magma that supplied the enclaves and dikes to suite I may also have provided the necessary heat to a thermally perturbed and thickened crust to initiate large-scale lower crustal melting.

The suite II rocks do not contain abundant mafic enclaves or dikes. The rocks are undeformed and preserve primary magmatic textures such as flow-aligned crystals and melt filled shears. Geochemical and Sr isotopic evidence show that AFC dominated processes produced the observed geochemical variation within suite II. Fractional crystallization of plagioclase, hornblende, sphene, apatite, and zircon with concurrent assimilation of a more isotopically evolved lithology adequately explains the data. The AFC trends developed in suite II are discontinuous with the trends of the more mafic suite I rocks indicating that the two suites are unrelated through any reasonable fractional crystallization scenarios. Utilizing the least evolved composition, we suggest that the parental magmas were generated by partial melting of amphibolitic lithologies at lower crustal pressure and temperature conditions.

Available field, geochemical and isotopic data indicate that similar magmatic processes as described for the QIC may also have affected other plutons of the GTS. The identification of structurally distinct sheets in the Carlson Creek and Mount Juneau suggests that they may be similar in origin to the QIC thus requiring a regionally extensive environment of partial melting and magma mixing.

References

Allen, C.M. 1991. Petrogenesis of the reversely zoned Turtle pluton, southeastern California. Ph. D. thesis, Virginia Polytechnic Institute and State University, Blacksburg, Virginia.

Arth, J. G., Barker, F. and Stern, T. W. 1988. Coast batholith and Taku plutons near Ketchikan,Alaska: Petrography, geochronology, geochemistry, and isotopic character. American Journal of Science, **288-A:** pp. 461-489.

Armstrong, R.L. 1988. Mesozoic and Cenozoic mamgatism of the Canadian Cordillera. *In* Processes in continental lithospheric deformation. *Edited by* S. P. Clarke, B. C. Burchfiel,and J. Suppe. Geological Society of America. Special Paper 218, pp. 55-91.

Armstrong, R.L. and Runkle, D. 1979. Rb-Sr geochronolmetry of Ecstall, Kitkiatka and Quottoon plutons and their country rocks, Prince Rupert region, Coast Plutonic Complex, British Columbia. Canadian Journal of Earth Science, **16:** 387-399.

Beard, J.S. and Lofgren, G.E. 1991. Dehydration-melting and water-saturared melting of basaltic and andesitic greenstones and amphibolites at 1, 3, and 6.9 kb. Journal of Petrology, **32:** 365-401.

Blundy, J. D., and Sparks, R. S. J. 1992. Petrogenesis of mafic inclusions of the Adamello massif, Italy. Journal of Petrology, **33:** 1039-1104.

Borsi, L., Petrini, R., Talarico, F. and Palmeri, R. 1995. Hgeochemistry and Sr-Nd isoptoes of amphibolite dykes from northern Victorialand, Antarctica. Lithos, **35:** 245-259.

Brew, D. A. 1994. Latest Mesozoic and Cenozoic magmatism in southeastern Alaska. *In* The Geology of Alaska. *Edited by* Plafker, G. and Berg, H. C. Geological Society of America, The Geology of North America, **G-1:** 621-656.

Brew, D. A. and Ford, A. B. 1978. Megalineament in southeastern Alaska marks southwest edge of the Coast Range batholithic complex. Canadian Journal of Earth Science, **15:** pp. 1763-1772.

Brew, D. A. and Ford, A. B. 1981. The Coast plutonic complex sill, southeastern Alaska. In: The Geological Society of America-Accomplishments during 1979. *Edited by* Albert, N. R. D. and Hudson, T. L. U. S. Geological Survey Circular **823-B:** B96-B99.

Brew, D. A. and Ford, A. B. 1983. Comment on Monger, J. W. H., Price, R. A., and Tempelman-Kluit, D. J. 1982. Tectonic accretion and the origin of two major metamorphic and plutonic welts in the Canadian Cordillera. Geology, **11:** pp. 427-429.

Crawford, M. L. and Hollister, L. S. 1982. Contrast of metamorphic and structural histories across the Work Channel Lineament, Coast Plutonic Complex, British Columbia. Journal of Geophysical Research, **87:** 3849-3860.

Crawford, W.L., Hollister, L.S., and Woodsworth, G.J. 1987. Crustal deformation and regional metamorphism across a terrane boundary, Coast Plutonic Complex, British Columbia. Tectonics, **6:** 343-361.

Defant, M. J., Clarke, L.F., Stewart, R.H., Drummond, M.S., de Boer, J.Z., Maury, R.C., Bellon, H., Jackson, T.E., and Restrepo, J.F. 1991. Andesite and dacite genesis via contrasting processes: the geology and geochemistry of El Valle Volcano, Panama. Contributions to Mineralogy and Petrology, **106:** 309-324.

Defant, M. J. and Nielsen, R. L. 1990. Interpretation of open system petrogenetic processes: phase equilibria constraints on magma evolution. Geochim Cosmochim Acta, **54:** pp. 87-102.

Desouuky, M. E., martin, F., and Mohr, P. 1996. Diorite-granite magma mingling and mixing along the axis of Galaway Granite batholith, Ireland. Journal of the Geologic Society, London. **153:** 361-374.

DePaolo, D. J. 1981. Trace element and isotopic effects of combined wallrock assimilation and fractional crystallization. Earth and Planetary Science Letters, **53:** pp. 189-202.

Dodge, F.C.W. and Kistler, R.W. 1990. Some additional observations of granitic rocks of the Sierra Nevada. Journal of Geophysical resolution, **95:** 17841-17848.

Drake, M. J. and Weill, D. F. 1975. Partitioning of Sr, Ba, Ca, Y, Eu^{2+}, Eu^{3+} and other REE between plagioclase feldspar and magmatic liquid: an experimental study. Geochimica et Cosmochimica Acta, **39:** 689-712.

Drinkwater, J. L.Brew, D. A. , and Ford, A. B. 1989. Petrographic and chemical description of the variably deformed Speel River pluton south of Juneau, southeastern Alaska. U. S. Geological Survey Bulletin **1903**, 104-112.

Drinkwater, J.L., Brew, D.A., and Ford, A.B. 1990. Petrographic and chemical data for the large Mesozoic and Cenozoic plutonic sills east of Juneau, southeastern Alaska. U. S. Geological Survey Bulletin **1918**, 47p.

Drinkwater, J.L., Brew, D.A., and Ford, A.B. 1995. Geology, petrography, and geochemistry of granitic rocks from the Coast Mountains Complex near Juneau, southteastern Alaska. U. S. Geological Survey Open-File Report **95-638**, 115 p.

Drummond, M.S. and Defant, M.J. 1991. A model for trondhjemite- tonalite-dacite genesis and crustal growth via slab melting: Archean to modern comparisons. Journal of Geopohysical research, **95:** 21503-21521.

Eberz, G.W. and Nicholls, I. A. 1990. Chemical modification of enclave magma by post-emplacement crystal fractionation, diffusion, and metasomatism. Contributions to Mineralogy and Petrology, **104:** 47-55.

England, P. C. and Thompson, A. B. 1984. Pressure-temperature-time paths of regional metamorphism, Pt. I. heat transfer during the evolution of regions of thickened crust. Journal of Petrology, **25:** 894-928.

Fujimaki, H. 1986. Partition coefficients of Hf, Zr, and REE between zircon, apatite and liquid. Contributions to Mineralogy and Petrology, **94:** 42-45.

Gareau, S. A. 1991. Geology of the Scotia-Qual metamorphic belt Coast Plutonic Complex, British Columbia. Ph.D. thesis, Carleton University, Ottawa, Ontario.

Gehrels, G. E. and McClelland, W. C. 1988. Earlt Tertiary uplift of the central and northern Coast Range batholith along west-side-up extensional shear zones. Geologic Society of America abstracts with programs, **20:** 111.

Gehrels, G.E., McClelland, W.C., Samson, S.D., Patchett, P.J., and Brew, D.A. 1991b. U-Pb geochronology and tectonic significance of late Cretaceous Early Tertiary plutons in the northern Coast Mountains batholith. Canadian Journal of Earth Sciences, v. **28**: 899-911.

Gill, J. B. 1981. Orogenic andesites and plate tectonics. Springer, Berlin.

Green, T. H. and Pearson, N. J. 1985a. Experimental determination of REE partition coefficients between amphibole and basaltic liquids at high pressure. Geochimica et Cosmochimica Acta, **49:** 1465-1468.

Hawkesworth, C.J., Gallagher, K., Hergt, J.M., and McDermott, F. 1994. Destuctive plate magmatism: Geochemistry and melt generation. Lithos, **33:** 169-188.

Hildreth, W. H. and Moorbath, S. 1988. Crustal contributions to arc magmatism in the Andes of central Chile. Contributions to Mineralogy and Petrology, **98:** 455-489.

Holden, P., Halliday, A. N., Stephens, W. E., and Heney, P. J. 1991. Chemical and isotopic evidence for major mass transfer between mafic enclaves and felsic magma. Chemical Geology, **92:** 135-152.

Hollister, L.S. 1982. Metamorphic evidence for the rapid (2 mm/year) uplift of a portion of the Central Gneiss Complex, Coast Mountains, British Columbia. Canadian Mineralogist, **20:** 319-332.

Hollister, L. S., Grissom, G. C., Peters, E. K., Stowell, H. H., and Sisson, V. B. 1987. Confirmation of the empirical correlation of Al in hornblende with pressure of solidification of calk-alkaline plutons. Ammerican Mineralogoist, **72:** 231-239.

Huppert, H. E. and Sparks, R. S. J. 1988. The fluid dynamics of crustal melting by injection of basaltic sills. Transactions of the Royal Society of Edinburgh, **79:** 237-243.

Hutchison, W.W. 1982. Geology of the Prince Rupert-Skeena map area, British Columbia, Geological Survey of Canada, memoir 394, 1-116.

Ingram, G. M. 1992. Deformation, emplacement and tectonic inferences: the Great Tonalite Sill, southeastern Alaska, U.S.A. Ph.D. thesis, University of Durham, Great Britain.

Irving, A. J. and Frey, F. A. 1978. Distribution of trace elements between garnet megacrysts and host volcanic liquids of kimberlitic to rhyolitic composition. Geochimica et Csomochimica Acta, **42:** 771-787.

Johnson, R. W. and Chappell, B. W. 1979. Chemical analyses of rocks from the late Cenozoic volcanoes of north-central New Britain and the Witu Islands, Papau, New Guinea. The Bureau of Mineral Resources of Australia Report **209**, BMR microform MF76.

Kay, R. W. 1978. Aleutian magnesian andesites: melts from Pacific Ocean crust. Journal of Volcanology and Geothermal Research, **4:** pp. 117-132.

Kenah, C. 1979. Mechanisms and physical conditions of emplacement of the Quottoon pluton, British Columbia. Ph.D. thesis, Princeton University, Princeton, New Jersey.

Klepeis, K. A. and Crawford, M. L. 1996. Structural history of the Coast shear zone near Portland Inlet, AK/BC. American Geophysical Union fall meeting abstracts with programs, **77:** n. 46, F652.

Langmuir, C.H., Vocke, R.D., Jr., and Hart, S.R. 1978. A general mixing equation with application to Icelandic basalts. Earth and Planetary Science Letters, **37:** 380-392.

Mason, D. R. 1987. Mix-n-Mac: a petrological least-squares mixing program. Glenside, Australia.

Meyers, J. D. and Sinha, A. K. 1983. Assimilation of crustal material by basaltic magma: strontium isotopic and trace element data from the Edgecumbe volcanic field, SE Alaska. Journal of Petrology, **25:** pp. 1-26.

Meyers, J.D. and Frost, C.D. 1994. A petrologic reinvestigation of the Adak volcanic center, central Aleutian arc, Alaska. Journal of Volcanology and Geothermal Research, **60:** 109-146.

Monger, J.W.H. 1993. Canadian Cordillera tectonics: From geosynclines to crustal collage. Canadian Journal of Earth Sciences, v. **30**, 209-231.

Monger, J. W. H., Price, R. A., and Templeman-Kluit, D. J. 1982. Tectonic accretion and the origin of two major metamorphic and plutonic welts in the Canadian Cordillera. Geology, **10:** pp. 70-75.

Patiño Douce, A. E., Johnston, A. D., and Humphreys, E. D. 1990. Closed system anatexis in the Cordilleran interior: the importance of initilal lithologic structure. EOS, **71:** 298-299.

Patiño Douce, A.E. and Beard, J.S. 1995. Dehydration-melting of biotite gneiss and quartz amphibolite from 3 to 15 kb. Journal of Petrology, **36:** 707-738.

Patterson, S. R., Vernon, R. H., and Tobisch, O. T. 1989. A review for the criteria for the identification of magmatic and tectonic foliations in granitoids. Journal of Structural Geology, **11:** 349-363.

Pearce, J. A. and Gale, G. H. 1977. Identification of ore-deposition environment from trace element geochemistry of associated igneous host rocks. Geological Society Special Publication, **7:** 14-24.

Pearce, J.A. and Peate, D.W. 1995. Tectonic implications of the composition of volcanic arc magmas. Annual Review of Earth and Planetary Sciences, **23:** 251-285.

Philpotts, J. A., and Schnetzler, C. C. 1970. Phenocryst-matrix partion coefficients for K, Rb, Sr and Ba with applications to anorthosite and basalt genesis. Geochimca et Cosmoshimica Acta, **34:** 307-322.

Ragland, P. C. 1989. Basic analytical petrology. Oxford Press, New York.

Rollinson, H. 1995. Using geochemical data: evaluation, presentation, interpretation. Longman Group Limited, UK.

Rubin, C. M., Saleeby, J. B., Cowan, D. S., Brandon, M. T., and McGoder, M. F. 1990. Regionally extensive mid-Cretaceous west vergent thrust system in the northwestern Cordillera: implications for continent-margin tectonism. Geology, **17:** 276-280.

Rushmer, T. 1991. Partial melting of two amphibolites: contrasting experimental results under fluid absent conditions. Contributions to Mineralogy and Petrology, **107:** 41-59.

Samson, S. D. 1990. Neodymium and Strontium isotopic characterization of the Wrangellia, Alexander, Stikine, Taku and Yukon crystalline terranes of the Canadian Cordillera. Ph. D. thesis, The University of Arizona, Tuscon.

Samson, S. D., Patchett, J.P., McClelland, M.C., and Gehrels, G.E. 1991. Nd and Sr constraints on the petrogenesis of the west side of the northern Coast Mountains batholith, Alaskan and Canadian Cordillera. Canadian Journal of Earth Sciences, **28:** 939-946.

Schmidt, M. W. 1992. Amphibole composition in tonalite as a function of pressure; an experimental calibration of the Al-in-hornblende barometer. Contributions to mineralogy and Petrology, **110:** 304-310.

Schnetzler, C. C. and Philpotts, J. A. 1970. Partition coefficients for rare earth elements between igneous matrix materials and rock forming mineral phenocrysts-II. Geochimica et Cosmochimica Acta, **34:** 331-340.

Shaw, D. M. 1970. Trace element fractionation during anatexis. Geochimca et Cosmochimica Acta, **34:** 237-243.

Sinha, A. K. and Davis, G. L. 1970. Geochemistry of the Franciscan volcanic and sedimentary rocks from California. *In* Carnegie Institution Year Book **69:** 394-397.

Sinha, A. K. and Thomas, J. B., Crawford, M. L., and Beard, J. S., 1996, The nature of Paleogene magmatism along the ACCRETE corridor, American Geophysical Union fall meeting abstracts with programs, **77:** n. 46, F652.

Sisson, T.W., and Grove, T.L. 1989. Water-saturated melting of low-magnesium andesite and basalt, revisited. EOS, **70:** 506.

Strekeisen, A. L. 1973. Plutonic rocks. Geotimes, **18:** 26-30.

Taylor, S. R. and McLennan, S. M. 1981. The composition and evolution of the continental crust: rare earth element evidence from sedimentary rocks. Philosophical Transactions of the Royal Society, **A301:** 381-399.

Thomas, J. B. and Sinha, A. K. 1997. The Quottoon Igneous Complex: a record of tectonic evolution along the Coast Shear Zone. Geological Society of America abstracts with programs, **29:** A-83.

Van der Heyden, P. 1989. U-Pb abd K-Ar geochronometry of the Coast Plutonic Complex, 53°N to 54°N, British Columbia, and implications for the Insular-Intermontane boundary. Ph.D. thesis, University of British Columbia.

Vernon, R.H. 1983. Restites, xenoliths and microgranitoids enclaves in granites. Journal and Proceedings, Royal Society of New South Wales, **116:** 77-103.

Watson, E. B. 1982. Basalt contamination by continental crust: Some experimental models. Contributions to Mineralogy and Petrology, **80:** 73-87.

Watson, E. B. and Jurwiez, S.R. 1984. Behavior of alkalis during diffusive interaction of granitic xenoliths with basic magma. Journal of Geology, **92:** 121-131.

Wendlandt, E., DePaolo, D. J. and baldridge, W. S. 1993. Nd and Sr chronostratigraphy of the Colorado Plateau lithosphere: implications for magmatic and tectonic underplating of the continental crust. Earth and Planetary Science Letters, **116:** 23-43.

Winther, K. T. 1996. An experimentally based model for the origin of tonalitic to trondhjemitic melts. Chemical Geology, 1**27:** 43-59.

Wolf, M.B. and Wyllie, P.J. 1994. Dehydration melting of amphibolite at 10 kb: the effects of temperature and time. Contributions to Mineralogy and Petrology, **115:** 369-383.

Wones, D. A. 1981. Mafic silicates as indicators of intensive variables in granitic magmas. Mining Geology, **31:** 191-212.

Wones, D. A. 1989. Significance of the assemblage titanite + magnetite + quartz in granitic rocks. American Mineralogist, **74:** 744-749.

Zen, E-an. 1988b. Thermal modelling of stepwise anatexis in a thrust-thickened sialic crust. Transactions of the Royal Society of Edinburgh, **79:** 223-235.

Appendix 1: Analytical Methods

Introduction

All sample preparations and analyses were performed at Virginia Tech by the author unless noted otherwise.

Electron Micrprobe

Major element compositions of minerals were determined with an automated Cameca SX-50 Electron Probe Microanalyzer. Accelerating voltage was 15 kV, and beam current 20 nA. Data from the probe was immediately reduced using the correction scheme of Ziebold and Ogilvie (1964), Bence and Albee (1986), and Albee and Ray (1970). Errors on individual analyses are assumed to be 2 standard deviations/mean for elements in the Kakanui hornblende, a mineral used in calibration of the machine. Eelemental abundances are on an oxygen basis. Analyses of minerals are listed in appendix 2.

Whole Rock Preparation

Fresh whole-rock samples weighing 5-20 kg (weight dependent on grain size) were reduced to <0.5 cm chips in a steel-faced jaw crusher and split to assure representative sampling. A portion of each sample (~150 g) was powdered in a tungsten carbide shatter box for $\leq$60 s to ~200 mesh. These powders were then used for major element, trace element, rare earth element, and Sr isotope analyses.

Major Element, Trace Element and Rare Earth Element Analyses

Major elements and trace elements were measured by fusion ICP-MS and Ba, Zr, and Nb by INAA at Activation Laboratories, Ontario, Canada. Rare earth element abundances for samples from the QIC were measured at Activation laboratories, Ontario Canada with an Elan-5000 ICP-MS.

Sr Isotope Analyses

All reagent grade HCl, HNO_3, HF, and H_2O used in dissolution and subsequent extraction of Sr were produced by subboiling distillation in teflon. Each unspiked whole-rock sample weighing 0.05 g was dissolved in a HF-HNO_3 mixture using 5 ml Savillex TFE dissolution bombs at ~100°C for 7 days on a hotplate. After complete dissolution, the HF-HNO_3 mixture was evaporated in laminar flow. The fluorides residue was converted to chloride by adding 6N HCl and evaporating to dryness. The samples were then equilibrated with 1 ml 2.5N HCl, and centrifuged in clean microcentrifuge tubes. The solution was then loaded onto a cation exchange column, which consisted of 0.5 cm diameter pyrex glass tube with a fitted blown silica frit, filled with 3 ml of AG 50x8, 200-400 mesh resin with a bed length of ~20 cm, previously washed with HCl and water, and conditioned with 2.5N HCl. After loading onto the column, the samples were eluted with 2.5N HCl. PMP beakers were cleaned in warm HCl bath and refluxed in warm teflon distilled 6N HCl prior to collection of Sr.

Sr samples were loaded as phosphates onto a degassed Re filament onto which a Ta_2O_5 slurry had been dried to produce a coating of the oxide. After the sample was loaded, the filament was heated to a dull red glow. The sample was then loaded into the turret and then into the mass spectrometer.

$^{87}Sr/^{86}Sr$ ratios were determined on an automated VG-54 mass spectrometer at VPI-SU. $^{87}Sr/^{86}Sr$ ratios during the run were corrected for fractionation using $^{86}Sr/^{88}Sr$ equal to 0.1194. The Sr_i was calculated using the crystallization age of 58.6 Ma (Gehrels et al., 1991). Replicant analyses (n=6) of the Eimer and Amend $SrCO_3$ standard gave a value of 0.70808 $\pm$7 (2σ) during the course of this work.

Appendix 2: Microprobe Analyses of Minerals

PLAGIOCLASE ANALYSES FOR SAMPLE 2093

SiO_2	Al_2O_3	TiO_2	FeO	CaO	Na_2O	K_2O	TOTAL
61.95	24.88	0.00	0.00	6.12	8.09	0.23	101.27
61.89	24.61	0.00	0.00	6.04	7.24	0.41	100.18
59.87	24.99	0.00	0.04	6.29	7.86	0.34	99.40
61.75	24.81	0.01	0.10	6.62	8.13	0.20	101.61
60.70	25.03	0.00	0.00	6.02	8.22	0.30	100.26
61.38	24.64	0.03	0.14	6.24	8.10	0.30	100.83
59.87	24.99	0.00	0.04	6.29	7.86	0.34	99.40
60.19	24.84	0.00	0.02	6.01	8.48	0.13	99.67

POTASSIUM FELDSPAR ANALYSES FOR SAMPLE 2093

SiO_2	Al_2O_3	TiO_2	FeO	MnO	MgO	CaO	Na_2O	K_2O	TOTAL
63.57	18.88	0.03	0.09	0.01	0.11	0.03	1.19	13.70	97.61
64.69	18.67	0.03	0.08	0.01	0.50	0.07	1.44	13.51	99.00

HORNBLENDE ANALYSES FOR SAMPLE 2093

SiO_2	Al_2O_3	TiO_2	FeO	MnO	MgO	CaO	Na_2O	K_2O	TOTAL
44.71	9.11	1.45	17.55	0.42	11.26	11.50	1.52	1.02	98.54
43.83	9.84	1.46	16.84	0.48	10.61	12.08	1.17	1.12	97.63
44.48	9.77	1.58	16.93	0.43	10.97	12.23	1.25	1.09	99.16
44.96	9.17	1.44	16.40	0.47	11.33	11.72	1.54	1.01	98.44
44.13	9.48	1.49	17.07	0.40	10.90	12.12	1.37	1.12	98.48
41.82	10.45	1.65	18.04	0.38	10.42	11.50	1.59	1.12	96.97

BIOTITE ANALYSES FOR SAMPLE 2093

SiO_2	$Al2O_3$	TiO_2	FeO	MnO	MgO	CaO	Na_2O	K_2O	TOTAL
35.32	15.19	3.96	18.16	0.21	11.20	0.02	0.09	9.05	93.21
35.48	14.80	4.06	19.06	0.30	11.04	0.02	0.08	8.99	93.83
37.25	14.67	4.05	18.46	0.29	11.62	0.05	0.05	8.92	95.36
36.89	14.77	4.14	18.72	0.30	11.29	0.05	0.06	8.90	95.12
36.88	14.74	4.25	18.36	0.21	11.78	0.06	0.07	9.06	95.40
36.19	14.19	4.00	18.51	0.27	11.16	0.11	0.11	8.86	93.39

APATITE ANALYSES FOR SAMPLE 2093

P_2O_5	SiO_2	TiO_2	Al_2O_3	Cr_2O_3	CaO	MnO	FeO	TOTAL
44.82	0.11	0.01	0.03	0.00	57.52	0.05	0.03	102.62
45.51	0.07	0.10	0.00	0.50	56.04	0.11	0.57	102.97

ILMENITE ANALYSES FOR SAMPLE 2093

P_2O_5	TiO_2	Al_2O_3	Cr_2O_3	MgO	CaO	MnO	FeO	TOTAL
0.08	12.37	0.14	0.27	0.03	0.29	0.24	75.56	89.09
0.07	12.37	0.15	0.25	0.03	0.29	0.27	75.76	89.26
0.00	45.46	0.02	0.00	0.39	0.02	1.22	48.92	96.07
0.07	43.86	0.02	1.03	0.05	0.07	1.07	50.90	97.07

MAGNETITE ANALYSES FOR SAMPLE 2093

P_2O_5	TiO_2	Al_2O_3	Cr_2O_3	MgO	CaO	MnO	FeO	TOTAL
0.06	0.22	0.11	1.05	0.01	0.23	0.12	90.72	92.52
0.10	0.21	0.09	0.73	0.02	0.22	0.13	90.93	92.43

Vita

Jay was born on October 1, 1970 in Roanoke, Virginia and was raised there. He attended Northside High School and then graduated from Guilford College in May of 1995 with a B.A. in geology. During his final year at Guilford he met A. K. Sinha at a meeting and decided to attend Virginia Tech. Since coming to Virginia Tech he has learned to run a clean lab at +100 conditions, operate a solid source thermal ionization mass spectrometer, electron microprobe, scanning electron microscope, all types of computers and their programs, cycled over some of the biggest mountains in Virginia, sliced through tall standing waves in many rivers, caught many smallmouth bass, and met some of the coolest people of his life. The knowledge of the earth that he gained through geology has allowed him to view the world with newfound eyes that are as young as the morning.